THE ASTROPHYSICAL JOURNAL, 462:183–202, 1996 May 1

NEW INSIGHTS INTO THE PHYSICAL NATURE OF LINERs FROM A MULTIWAVELENGTH ANALYSIS OF THE NUCLEUS OF M81[1]

LUIS C. HO[2] AND ALEXEI V. FILIPPENKO
Department of Astronomy, University of California, Berkeley, CA 94720
AND
WALLACE L. W. SARGENT
Palomar Observatory, Caltech 105-24, Pasadena, CA 91125
Received 1995 April 10; accepted 1995 August 8

ABSTRACT

We discuss the physical conditions and excitation of the nucleus of M81 by combining ground-based optical spectra, archival *Hubble Space Telescope* (*HST*) ultraviolet (UV) and optical spectral, and published X-ray measurements. This well-known low-ionization nuclear emission-line region (LINER) is representative of a general class of objects thought to be the less luminous counterparts of active galactic nuclei (AGNs) present in Seyfert galaxies and quasars. A featureless UV continuum, most likely of nonstellar origin, is detected unambiguously for the first time in M81. Compared with "classical," more luminous AGNs, the UV continuum is weak relative to the X-rays, the slope between 1200 and 3000 Å is significantly steeper ($f_\nu \propto \nu^{-2.0\pm0.3}$ rather than $\nu^{-0.5}$ to ν^{-1}), and the "big blue bump" is absent. The nonstellar continuum of the nucleus has an absolute blue magnitude of -11.6, only a factor of 5 brighter than that of the least luminous Seyfert 1 nucleus in NGC 4395. We suggest that these characteristics of the spectral energy distribution may be a generic property of galactic nuclei having low-level activity, perhaps being a manifestation of extremely low accretion rates. The UV-optical spectrum exhibits broad emission lines with FWHM ≈ 2500 km s^{-1}, further reinforcing the similarity to Seyfert 1 nuclei.

Detailed properties have been derived for the regions emitting narrow and broad lines. The narrow-line region is characterized by velocities of 200–1000 km s^{-1}, a large, radially decreasing gradient in density ranging from a few times 10^2 to 10^7 cm^{-3}, and a spatial extent of less than 1 to several parsecs from the central ionizing source. We deduce that the gas has roughly solar metallicity, an ionization parameter of $\sim 10^{-3.3}$, and electron temperatures typical of photoionized nebulae. Lacking information on the structure of the broad-line region, we can obtain only crude estimates of its density (10^9–10^{10} cm^{-3}), ionization parameter ($\lesssim 10^{-2.8}$), and radius (0.001–0.004 pc).

Combining the velocities and dimensions of the broad-line region, and assuming that gravity dominates the motions of the clouds, we derive a central mass of (0.7–3) $\times 10^6\ M_\odot$ for the nucleus of M81. The low bolometric luminosity of the nucleus implies that it is radiating only at (2–10) $\times 10^{-4}$ of the Eddington limit.

Our extensive ground-based monitoring reveals that the broad component of the Hα emission line has not varied significantly during the past 15 yr, although X-ray variability on timescales of years has been reported. This variability pattern is not yet understood. The broad Hα luminosity (1.8×10^{39} ergs s^{-1}) is 15 times larger than in NGC 4395, assuming that the reddening intrinsic to the broad-line region is negligible in both objects.

Subject headings: galaxies: individual (M81) — galaxies: nuclei — galaxies: Seyfert — line: profiles — spectrophotometry — ultraviolet: spectra

1. INTRODUCTION

The active galactic nucleus (AGN) phenomenon extends over an enormous range in luminosity (e.g. Filippenko 1989). Although "classical" AGNs were originally defined by luminous objects such as quasars and type 1 Seyfert galaxies, it is now established that much less powerful sources manifest similar observed properties. Several spectroscopic surveys (Heckman 1980; Stauffer 1982; Keel 1983; Filippenko & Sargent 1985; Phillips et al. 1986; Ho, Filippenko, & Sargent 1995) reveal that a large fraction of nearby galaxies exhibit emission-line properties that apparently cannot be accounted for by normal stellar processes (Ho, Filippenko, & Sargent 1996). Most of these objects belong to a class known as "low-ionization nuclear emission-line regions" (LINERs; Heckman 1980), whose optical spectra are characterized by strong, low-ionization forbidden lines of [O II], [O I], [N II], and [S II]. Although the dominant source of energy in typical LINERs is still under debate (see discussions in Filippenko 1993, Ho, Filippenko, & Sargent 1993, and Shields 1994), some objects, such as the nucleus of M81 (NGC 3031),[3] show a close resemblance to classical type 1 Seyfert nuclei.

[1] Based on observations with the NASA/ESA *Hubble Space Telescope*, obtained from the data archive at the Space Telescope Science Institute, which is operated by the Association of Universities for Research in Astronomy, Inc., under NASA contract NAS5-26555. Also based on data taken at Palomar Observatory (California Institute of Technology) and Lick Observatory (University of California).

[2] Present address: Harvard-Smithsonian Center for Astrophysics, 60 Garden Street, MS-42, Cambridge, MA 02138.

[3] The nucleus of M81 does not, strictly speaking, satisfy both of Heckman's (1980) criteria for a LINER ([O II] λ3727 > [O III] λ5007, and [O I] λ6300 > 0.33[O III] λ5007). According to the relative fluxes given in Ho et al. (1993), [O II] $\approx$ [O I] $\approx$ 0.85[O III]. Since strict boundaries are to some extent arbitrary, and there is little doubt that the ionization parameter of M81 is low (relative to Seyfert nuclei), we will classify M81 as a LINER.

As summarized in previous studies (Filippenko & Sargent 1988, hereafter FS; Fabbiano 1988; Keel 1989), the observed properties which make the nucleus of M81 one of the best candidates for a low-luminosity AGN include the presence of a broad component of the Hα emission line (Peimbert & Torres-Peimbert 1981; Shuder & Osterbrock 1981), a compact radio core (Bartel et al. 1982; Bietenholz et al. 1996), a pointlike X-ray source (Fabbiano 1988; Petre et al. 1993), and probable rapid X-ray variability (Barr et al. 1985). The broad Hα luminosity of the nucleus of M81 (FS) is a factor of 20 fainter than that of the lowest luminosity classical Seyfert 1 nucleus in NGC 4051 (Véron 1979).

The availability of archival spectra from the *Hubble Space Telescope* (*HST*), as well as published X-ray data from *ROSAT* and *BBXRT* (Petre et al. 1993), prompted us to reconsider several long-standing issues related to the nucleus of M81. In this paper, we combine these space-based data with ground-based spectra from our own extensive monitoring program. A summary of the available data sets is given in § 2, their analysis is detailed in § 3, and the results are discussed in § 4. Section 5 summarizes our main conclusions.

2. SUMMARY OF SPECTROSCOPIC DATA SETS

2.1. *HST Spectra*

The *HST* spectra used in this study are nonproprietary, Cycle 3 data obtained from the archive. Both UV and optical spectra of the nucleus of M81 were obtained with the Faint Object Spectrograph (FOS; Kinney 1994) using a 0.″3 round aperture. Two exposures (each 1500 s) were acquired on 1993 April 5 and 6 UT with the G130H grating and the blue Digicon (1152–1608 Å, 1.0 Å diode^{-1}). In addition, spectra were obtained on 1993 April 14 UT with the G270H (2222–3277 Å, 2.1 Å diode^{-1}), G400H (3235–4779 Å, 3.0 Å diode^{-1}), and G570H (4569–6818 Å, 4.4 Å diode^{-1}) gratings and the red Digicon, with exposure times of 2000, 1500, and 1500 s, respectively. The flux and wavelength scales of the spectra were calibrated by the staff at the Space Telescope Science Institute (STScI) in the normal manner. The two G130H spectra were combined. Unfortunately, no observations were taken with the G190H grating, resulting in a gap in the spectral coverage between 1608 and 2222 Å. The region of overlap between the G270H and G400H gratings showed excellent agreement in the relative fluxes, continuum shapes, and wavelength scale. The G570H spectrum, however, proved to be unusable. The region overlapping with the G400H spectrum shows a severe discrepancy in the flux level, and the overall spectrum has a much lower signal-to-noise ratio (S/N) than the spectra from the other gratings. The most likely explanation for this discrepancy is that the aperture was not properly centered on the nucleus during the G570H exposure.

The wavelength scales of the FOS gratings have a non-negligible zero-point offset resulting from misalignment of the FOS filter wheel (A. Koratkar 1995, private communication). We adjusted the zero point of the G130H spectrum using the narrow geocoronal Lyα line, and we shifted the G270H spectrum in such a way that the (Galactic) interstellar Lyα and Mg II λ2800 absorption lines coincided in velocity (see Appendix). The wavelengths of the narrow lines in the G400H spectrum showed good agreement with the ground-based data.

Figure 1 displays the final spectra. To slightly improve the S/N, we rebinned them in such a way that each pixel corresponds to the width of a single diode (1, 2, and 3 Å for the G130H, G270H, and G400H gratings, respectively). The S/N per diode in the continuum is approximately 4, 15, and 20, respectively. The G130H spectrum (Fig. 1*a*) shows prominent Lyα (both geocoronal and intrinsic to M81) and C IV λ1549 emission, as well as several weaker lines. Strong C II] λ2326, Mg II λ2800, and broad emission complexes due to Fe II dominate the G270H spectrum (Fig. 1*b*). The G400H spectrum (Fig. 1*c*), encompassing the near-UV region, contains the Balmer series in emission and the familiar optical forbidden emission lines. Remarkably, starlight contributes a minor fraction of the flux, even in the spectral range covered by the G400H grating, where ground-based observations are dominated by light from late-type stars. However, because the data were taken prior to the *HST* refurbishment mission, we expect the nucleus to contain some starlight contamination due to the aberrated point-spread function (PSF).

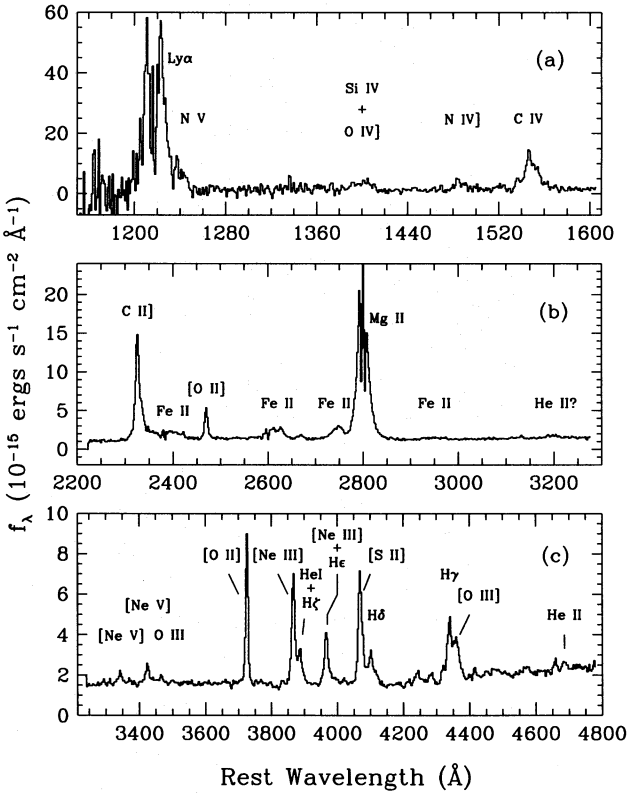

FIG. 1.—FOS spectra of the nucleus of M81 obtained with (*a*) the G130H grating on the blue side, as well as (*b*) the G270H and (*c*) the G400H gratings on the red side. The spectra were rebinned on a linear scale with a pixel size corresponding to the width of a single diode (1, 2, and 3 Å for the G130H, G270H, and G400H gratings, respectively). The main emission lines are labeled in each panel. The abscissa shows the rest wavelength after removing a radial velocity of −28 km s^{-1}.

2.2. *Ground-based Spectra*

Most of the optical spectra were obtained during the course of an extensive spectroscopic survey of nearby galaxies conducted with the double spectrograph (Oke & Gunn 1982) on the Hale 5 m telescope at Palomar Observatory (Filippenko & Sargent 1985; Ho et al. 1995); a small fraction of the data was acquired with the "UV Schmidt" spectrograph (Miller & Stone 1987) and the Kast spectrograph (Miller & Stone 1993) on the Shane 3 m reflector at

Lick Observatory. We took observations at multiple epochs primarily to monitor the variability of the broad component of the Hα emission line. Although FS and Ho et al. (1995) gave extensive accounts of the Palomar data, we summarize the salient features of the observations in Table 1 for the sake of completeness. Details of the instrumental setup, observation strategy, and data reduction can be found in the above references and will not be repeated here. The majority of the spectra cover the region 4220–5090 Å with 4 Å resolution (as determined from the full width at half-maximum [FWHM] of the wavelength comparison lines) and 6210–6860 Å with 2.5 Å resolution. To cover the entire observable optical bandpass, we extended the wavelength coverage from 3100 to 9800 Å with somewhat lower dispersion (5–8 Å). One of the low-resolution spectra was published by Ho et al. (1993). In all cases, one-dimensional spectra were obtained with an effective extraction width of 4″ along the slit.

3. DATA ANALYSIS

3.1. *The Emission-Line Spectrum*

3.1.1. *The FOS Spectra*

We removed the continuum from the FOS spectra by fitting a low-order spline function through several regions relatively uncontaminated by emission lines. For the G130H spectrum, we chose the regions 1280–1360, 1410–1460, and 1580–1600 Å. Broad Fe II emission produces undulations and mimics the continuum for a large portion of the G270H spectrum. The "continuum" level between C II] and Mg II (Fig. 1*b*), for instance, is elevated from the continuum blueward and redward of these lines, respectively. We used the regions 2225–2290, 2882–2914, 3010–3100, and 3235–3275 Å to fit the true continuum. Finally, we note that the inflection of the continuum shape of the G400H spectrum near 4200 Å is produced by a combination of stellar absorption from molecular bands (CN and CH), an increasing contamination from late-type stars at longer wavelengths and the contribution of the "small blue bump" (Wills, Netzer, & Wills 1985) rising shortward of about 3600 Å (§ 3.3). We removed the general curvature of the continuum but did not correct for the residual stellar absorption.

3.1.2. *The Ground-based Spectra*

Light from late-type stars contributes significantly to the ground-based optical spectrum of M81. In order to measure reliably the emission-line spectrum, the starlight contamination must be removed carefully. An effective technique uses a pure absorption-line galaxy as a "template" to model the stellar component. Thorough discussions of this method can be found in Filippenko & Halpern (1984), FS,

TABLE 1

JOURNAL OF GROUND-BASED OBSERVATIONS OF M81

UT Date	Start	Exp. (s)	P.A.[a] (deg.)	P.P.A.[b] (deg.)	Slit[c] (″)	Spectral Range (Å)	$\Delta\lambda$[d] (Å)	sec z[e]	Seeing[f] (″)	Tel.[g]	Weather
1984 Feb 12	04:52	600	65	64	2	4195 – 5300; 6240 – 6885	2.5;4	1.42	2 – 2.3	P5	Cloudy
1984 Feb 12	05:07	1500	65	58	2	4195 – 5300; 6240 – 6885	2.5;4	1.38	2 – 2.3	P5	Cloudy
1986 Feb 18	05:20	950	45	48	2	4215 – 5080; 6210 – 6858	2.5;4	1.32	3 – 4	P5	Cloudy
1986 Feb 25	04:19	600	60	59	4	4222 – 5088; 6210 – 6858	2.5;4	1.38	2 – 3	P5	Clear
1986 Feb 25	06:59	1500	0	4	1	4222 – 5088; 6210 – 6858	2.5;4	1.23	1 – 1.5	P5	Clear
1986 Feb 25	07:32	1000	138	174	1	4222 – 5088; 6210 – 6858	2.5;4	1.23	1 – 1.3	P5	Clear
1986 Feb 25	07:52	1100	48	166	1	4222 – 5088; 6210 – 6858	2.5;4	1.24	1 – 1.5	P5	Clear
1986 Feb 25	08:13	400	65	161	2	4222 – 5088; 6210 – 6858	2.5;4	1.25	1 – 1.5	P5	Clear
1986 Feb 25	08:22	1100	90	156	1	4222 – 5088; 6210 – 6858	2.5;4	1.25	1 – 1.3	P5	Clear
1986 Mar 27	02:59	300	65	48	2	4220 – 5090; 6210 – 6860	2.5;4	1.33	0.8 – 1	P5	Clear
1986 Mar 27	03:07	300	45	46	4	4220 – 5090; 6210 – 6860	2.5;4	1.31	0.8 – 1	P5	Clear
1986 Mar 29	05:49	960	65	166	2	4220 – 5090; 6210 – 6860	2.5;4	1.24	1 – 1.3	P5	Cloudy
1987 Jan 23	09:53	475	65	172	2	4230 – 5090; 6210 – 6850	2.5;4	1.24	1 – 1.3	P5	Cloudy
1987 Jan 24	09:46	400	65	173	2	4230 – 5090; 6210 – 6850	2.5;4	1.23	1.5	P5	Clear
1987 Feb 22	05:02	600	65	50	2	4220 – 5085; 6210 – 6860	2.5;4	1.33	1.5	P5	Cloudy
1987 Feb 22	05:16	1200	65	44	2	4220 – 5085; 6210 – 6860	2.5;4	1.31	1.5 – 2	P5	Cloudy
1988 Feb 08	03:12	400	65	94	2	4250 – 5125; 6215 – 6860	2.5;4	1.76	3	P5	Clear
1988 Feb 10	04:41	400	65	70	2	4250 – 5125; 6215 – 6860	2.5;4	1.46	1	P5	Clear
1988 Feb 10	04:49	200	65	68	4	4250 – 5125; 6215 – 6860	2.5;4	1.45	1	P5	Clear
1988 Apr 06	07:25	400	65	125	2	4250 – 5090; 6210 – 6850	2.5;4	1.36	2 – 2.5	P5	Clear
1988 Apr 07	03:09	300	65	31	2	4220 – 5090; 6210 – 6850	2.5;4	1.27	< 1	P5	Cloudy
1988 Apr 07	03:16	200	65	29	4	4220 – 5090; 6210 – 6850	2.5;4	1.26	< 1	P5	Cloudy
1988 Apr 09	03:04	400	65	30	2	4220 – 5090; 6210 – 6850	2.5;4	1.26	0.7	P5	Clear
1988 Apr 09	03:13	300	65	27	4	4220 – 5090; 6210 – 6850	2.5;4	1.26	0.7	P5	Clear
1990 Feb 10	07:42	600	19	12	1	4230 – 5110; 5030 – 7480	2.5;8	1.24	1.5	P5	Clear
1990 Feb 10	07:56	100	19	9	1	4230 – 5110; 5030 – 7480	2.5;8	1.24	1.5	P5	Clear
1990 Feb 11	07:39	600	19	12	1	3380 – 5070; 7380 – 9830	5;8	1.24	2	P5	Cloudy
1990 Nov 28	10:14	200	60	59	2	3480 – 5160; 5030 – 7480	5;8	1.38	1	P5	Clear
1990 Nov 29	09:55	300	60	63	2	3480 – 5160; 7380 – 9830	5;8	1.40	2 – 3	P5	Clear
1991 Apr 19	04:35	1300	170	162	2	6055 – 6810	3	1.24	1 – 1.5	L3	Cloudy
1992 Sep 21	13:07	300	90	83	2	3158 – 5280; 5822 – 7320	5;8	1.59	1.5	L3	Clear
1993 Apr 14	08:41	400	99	97	2	3112 – 5220; 6014 – 8040	5;8	1.59	1.5 – 2	L3	Cloudy

[a] Position angle of slit through the nucleus.
[b] Parallactic position angle at the midpoint of the observation.
[c] Slit width.
[d] Spectral resolution (FWHM).
[e] Secant of zenith angle (~ air mass) at the midpoint of the observation.
[f] Visual estimate of the seeing disk (FWHM in seconds of arc).
[g] P5 = Palomar 5 m. L3 = Shane 3 m.

Ho et al. (1993), and Ho et al. (1996). In our previous detailed study of M81 (FS), we used NGC 4339 as the template galaxy; however, Ho et al. (1996) found that NGC 4461 provides a better match to the velocity dispersion and metallicity of the stellar population. Consequently, we adopt NGC 4461 for the high-resolution (2.5–4 Å) data; for the low-resolution (5–8 Å) spectra, NGC 4461 was not available, so we used NGC 4339.

Measurement of weak, broad emission lines (§ 3.2) can be affected by a number of systematic errors. In addition to the general difficulty associated with removal of the strong stellar background, one must contend with potential errors in the shape of the continuum, both for the object of interest and for the template(s) used in the starlight subtraction. Mismatches between the continuum shape of the object and template can introduce low-frequency wiggles easily mistaken for genuine broad spectral features. The accuracy of the continuum shape depends on the reliability of the sensitivity function derived from calibration stars. Our experience with the double spectrograph on the Palomar 5 m telescope indicates that temporal variations in the spatial focus of the CCD sometimes introduce low-frequency undulations in the sensitivity function of the red spectra (Ho et al. 1995). However, during the observing runs of interest, it appears that, with the exception of one epoch (1988 April 9 UT), this effect is minimal. No spurious features resembling the well-known broad component of the Hα line are seen in the starlight-subtracted red spectra.

Since one of our aims is to quantify the variability of the broad Hα line, the spectra from each epoch were analyzed independently. Prior to performing the starlight subtraction, multiple exposures from the same night were combined in a weighted average, with the weights determined by the S/N of the individual exposures. We did not combine multiple exposures taken with different instrument setups (e.g., different slit width or position angle). In total, there are 28 spectra taken over 18 epochs. The starlight subtraction procedure was applied uniformly to all the spectra using the automated algorithm described in Ho et al. (1996).

3.1.3. *Photometric Scale*

To place the ground-based emission-line spectra on a common absolute flux scale, we determined the zero point by measuring the fluxes of several prominent forbidden lines from spectra taken with a wide (4″) slit on nights which were deemed to be photometric (see Table 1). We implicitly assume that forbidden lines do not vary over the timescale spanned by our observations. For the blue region, we chose [O III] λ5007 as the fiducial line for scaling, while [O I] λ6300 was used for the red region. Although somewhat weaker than the [S II] λλ6716, 6731 doublet, [O I] was favored because we expect it to originate from a smaller spatial scale than [S II] (§ 4.3.1), and thus it should be less affected by variations in the atmospheric seeing. The final flux scale, to within observational uncertainties, is similar to that found by FS, which we simply adopt in this study. We scaled each starlight-subtracted spectrum according to the fluxes of the fiducial lines.

The large difference between the effective apertures of the FOS and ground-based measurements greatly complicates quantitative comparison of fluxes between the two data sets. Assuming a distance of 3.6 Mpc for M81 (Freedman et al. 1994), the 0.″3 aperture samples a region of radius 2.7 pc around the nucleus; this dimension probably encloses the entire broad-line region (BLR) but only the inner portion of the narrow-line region (NLR). Since the NLR in M81 is known to be stratified in density (FS), with emission from lines of higher critical density coming from smaller radii, the fraction of the total narrow-line emission detected by the FOS aperture varies depending on the line in question. Indeed, we find that the FOS detected only $\sim\frac{1}{3}$ of the [O II] λ3727 flux measured from the ground-based data, whereas most of the flux from [S II] λλ4069, 4076, which has a much higher critical density compared to [O II] λ3727, was detected. Thus, in this paper, we will not derive quantitative results that make use of narrow-line fluxes measured from the different apertures, but we will assume that the broad lines are unaffected by aperture dilution. Unfortunately, the broad lines in the region of overlap between the FOS and ground-based spectra are weak and difficult to measure (§ 3.3), and we cannot easily verify the latter assumption.

To partially compensate for the gap in the *HST* spectral coverage (1608–2222 Å), we include in our analysis a few additional lines (O III] λ1663, N III] λ1750, Si III] λ1882, and C III] λ1909) measured from spectra obtained from the *International Ultraviolet Explorer* (*IUE*) archive. Comparison of lines detected in common by *HST* and *IUE* revealed that the fluxes of C IV and C II] show excellent agreement between the two instruments, differing by less than 8%. The Mg II flux as measured by *HST*, however, is at least twice that obtained with *IUE*; we attribute this discrepancy to the severe contamination of stellar absorption in the vicinity of Mg II due to the large *IUE* aperture (see, for example, the spectrum of M81 published by Kinney et al. 1993). We expect the spectral range between 1608 and 2222 Å to be much less affected by stellar absorption, and we take at face value the *IUE* fluxes in this region.

3.1.4. *Correction for Scattered Light*

UV spectra obtained with the FOS, particularly for the short wavelengths of the G130H grating, suffer from contamination by scattered light if the intrinsic spectrum of the source is very red (Rosa 1994). The G130H spectra were recalibrated using new STScI pipeline reduction software that empirically corrects the background and scattered light using the diode array shortward of 1150 Å; the newly calibrated data were kindly made available to us by G. A. Kriss.

3.1.5. *Comparison between FOS and Ground-based Spectra*

The wavelength coverage of the G400H spectrum overlaps with the ground-based spectra between 3480 and 4779 Å, and thus allows a direct comparison between data taken with very different angular resolution. The ability of the small FOS aperture to isolate the compact nuclear component from the surrounding, extended stellar background, despite the presence of spherical aberration, is dramatically illustrated in Figure 2. Suppressing the diffuse stellar background greatly enhances the detectability of the emission-line component. With the exception of small residuals from CN (~3810 Å), CN and Fe I (4140–4200 Å), and the G band (4300 Å), the G400H spectrum appears to be largely devoid of starlight. Although the apparent lack of stellar absorption features can be misleading, since velocity broadening in the nucleus can mimic dilution of the line strengths, the featureless, nonstellar continuum of the G270H and G130H spectra can be described fairly well by a single power-law function (§ 4.1), and extrapolation of this function reveals

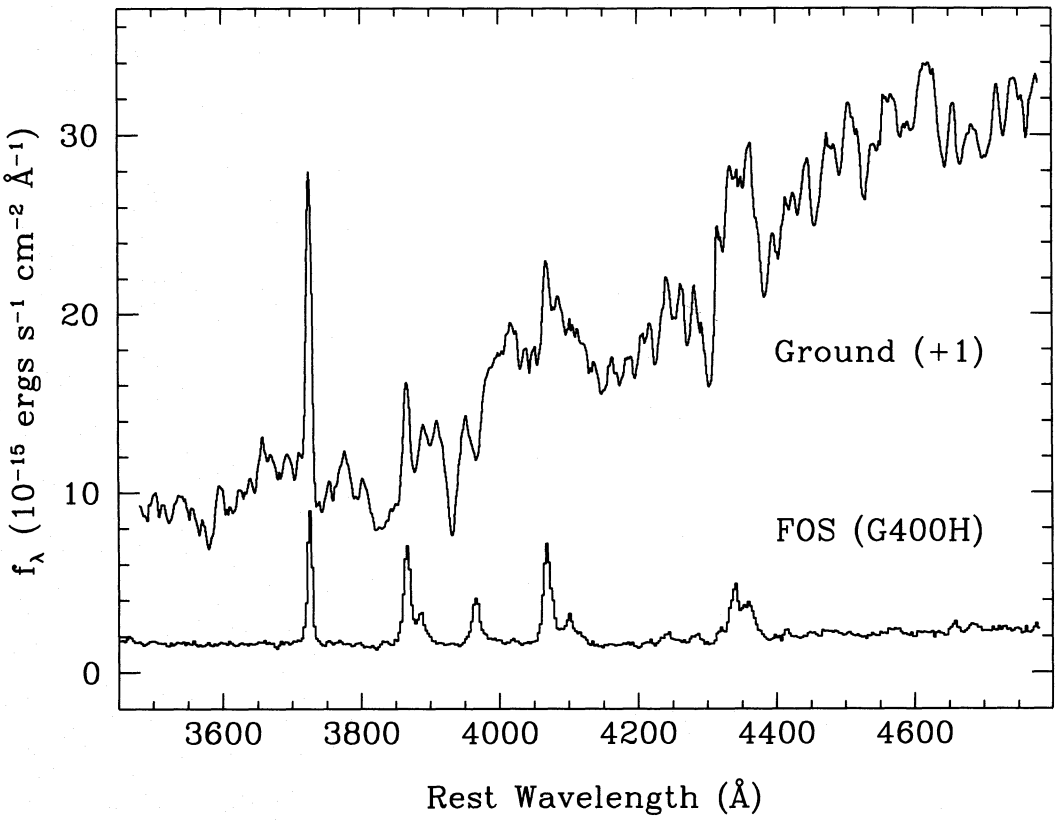

FIG. 2.—Ground-based and G400H spectra of the nucleus of M81 over the interval where the two wavelength regions overlap (3480–4779 Å). Both spectra are on the same flux scale, and the ground-based spectrum was offset by +1 unit in the ordinate for clarity. Note the dramatic improvement in the detectability of the emission lines in the G400H spectrum.

that the nonstellar component accounts for most of the continuum flux in the G400H spectrum. With the 0.″3 aperture, we find that starlight contributes only 7% and 15% to the continuum in the *U* (3500 Å) and *B* (4350 Å) bands, respectively. By comparison, we estimate that in the ground-based spectrum, taken from an effective aperture of 2″ × 4″, the fractional contribution from starlight to the continuum amounts to 73% in *U* and 92% in *B*.

Comparing the continuum-subtracted G400H spectrum with the starlight-subtracted ground-based spectrum provides yet another striking contrast (Fig. 3). In the ground-based spectrum, the region between 3480 and 4250 Å was obtained from a weighted average of three low-resolution spectra, while the section from 4250 to 4779 Å represents a weighted average of 16 high-resolution spectra with the best S/N. Despite the much longer effective integration time, the S/N of the ground-based spectrum pales by comparison with that of the FOS. The latter is not affected by residuals from imperfect starlight subtraction, enabling much more accurate measurement of line fluxes and profiles. Note in particular the unambiguous detection of the broad component of the Balmer emission lines, as well as the diagnostically important [O III] λ4363 line.

3.2. *Light Curve for* Hα

Our ground-based data set extends over a decade and allows us to examine the long-term variability of the broad Hα line. Since previous studies (e.g., FS) have concluded that Hα does not seem to vary, it is crucial that the entire data set be treated in a uniform manner so as not to obtain spurious results (see § 3.1.2). Severe blending with narrow Hα and [N II] λλ6548, 6583 complicates measurement of the broad Hα line. To facilitate handling of the large number of spectra, we simply measured the entire Hα+[N II] complex by summing the flux over the interval 6492–6659 Å in the starlight-subtracted spectra. Since we expect the narrow lines to remain constant, any potential variability would be attributed to the broad component of Hα, which accounts for more than 50% of the flux of the whole blend. The adopted wavelength range of integration corresponds to a full width near zero intensity (FWZI) of 7600 km s^{-1} for Hα, slightly larger than that found by FS (6900 km s^{-1}). We also measured several other lines to assess the reality of any potential variability and to evaluate the *intrinsic* scatter due to slit losses.

Figures 4*a*–4*c* show the light curves for [S II], Hα+[N II], and Hβ, respectively. Multiple observations taken on the same epoch were averaged. The ordinate displays the fluxes of individual epochs normalized to the median flux for the entire data set. The data should scatter randomly around unity if there is no variability. Several points deserve attention. (1) The amount of variation in the [S II] light curve (∼10%; Fig. 4*a*) is a reasonable measure of the magnitude of intrinsic scatter that could arise from a combination of slit losses and variations in the centering of the nucleus among different observing epochs. (2) If we exclude the single deviant point in the Hα+[N II] light curve (Fig. 4*b*), which is probably too high because of calibration complications (§ 3.1.2), it is apparent that the broad component of Hα does not exhibit any significant variability. The scatter of the fluxes about the median is approximately 10%–15%, only slightly larger than that of [S II] and consistent with the difficulty associated with measuring broad spectral features. (3) Finally, the much larger scatter (up to

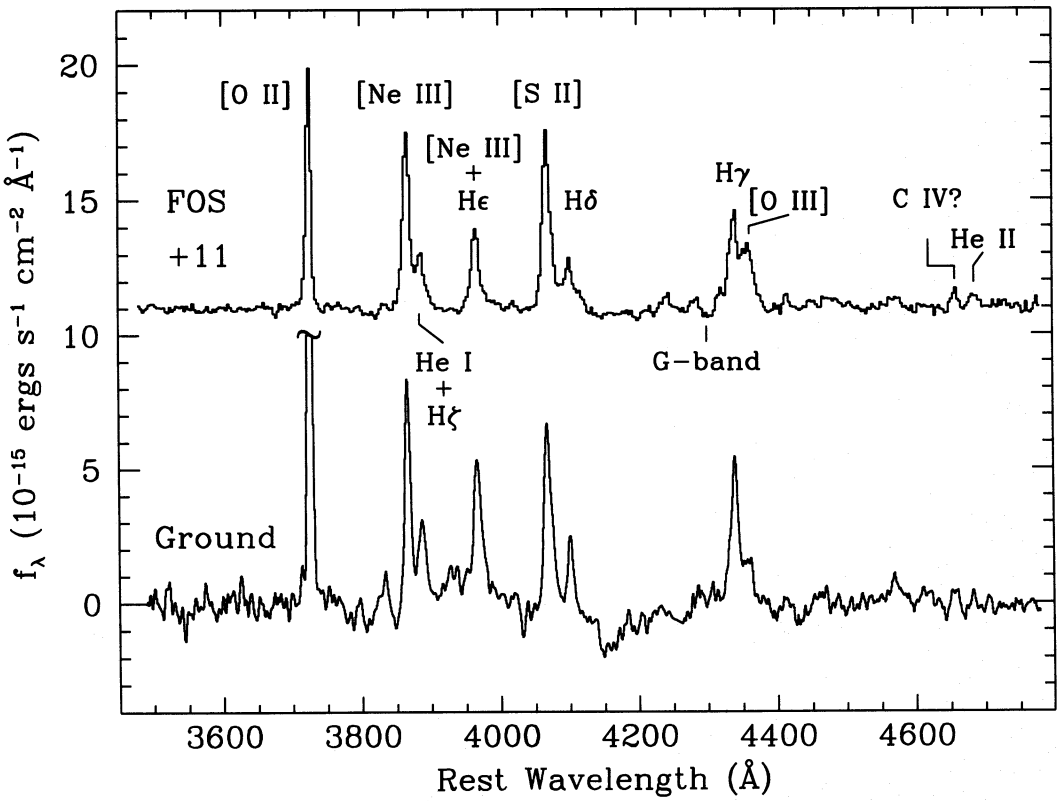

FIG. 3.—Comparison between the continuum-subtracted G400H spectrum (*top*) and the starlight-subtracted ground-based spectrum (*bottom*) over the region where the two overlap (3480–4779 Å). Both spectra are on the same flux scale, and the G400H spectrum was offset by +11 units in the ordinate for clarity. The main emission lines present in this region are labeled. In the ground-based spectrum, the section 3480–4250 Å was obtained from a weighted average of three low-resolution spectra, while the interval 4250–4779 Å represents a weighted average of the 16 high-resolution spectra with the best S/N. Note the superior quality of the G400H spectrum and the unambiguous detection of a broad component to the Balmer emission lines.

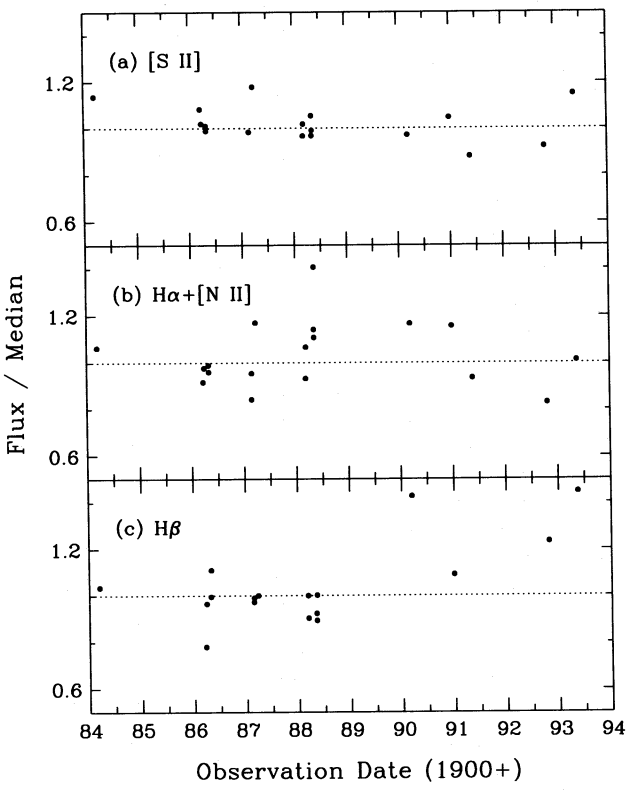

FIG. 4.—Light curves of the nucleus of M81 measured for (*a*) [S II] λλ6716, 6731 (6705–6743 Å), (*b*) the Hα+[N II] complex (6492–6659 Å), and (*c*) Hβ (4795–4925 Å). Multiple observations taken during the same epoch were averaged. The ordinate shows the ratio of the observed flux to the median value. The dashed line in each panel denotes unity.

40%) of Hβ (Fig. 4*c*) can be attributed entirely to the large uncertainty in the measurement of the low-resolution spectra taken between 1990 and 1993. If we consider only the 1984–1988 measurements, the amount of scatter is comparable to that of Hα.

3.3. *Measurement of Emission Lines*

We measured fluxes and profiles for all emission lines in the continuum-subtracted (FOS) and starlight-subtracted (ground-based) spectra. Whenever possible, the lines were fitted with Gaussians, but several cases required more involved treatment.

The Lyα profile (Fig. 5*a*), though fairly symmetric, is quite complicated, consisting of at least three components: broad emission, interstellar absorption, and, because of the small systemic velocity of M81 (−28 km s^{-1}; de Vaucouleurs et al. 1991), geocoronal emission. Undoubtedly a component from the NLR must also be present, but it is impossible to extract it from the complex profile. A rough estimate of the intrinsic emission profile was obtained by fitting Gaussians with various fixed heights and FWHMs, with the weak N v λ1240 line on its red wing constrained to have the same FWHM. The latter assumption is reasonable because both lines originate from the same region in the BLR (e.g., Kwan & Krolik 1981), and indeed, at least in NGC 5548, is supported by observations (Krolik et al. 1991). The best combination of parameters was determined subjectively by examining the residuals. It appears that a Gaussian with FWHM ≈ 4000 km s^{-1} provides a satisfactory fit. The base of the Lyα line, as judged by the extension of its blue wing, has FWZI ≈ 10,000 km s^{-1}.

The C IV λ1549 line also has interesting structure

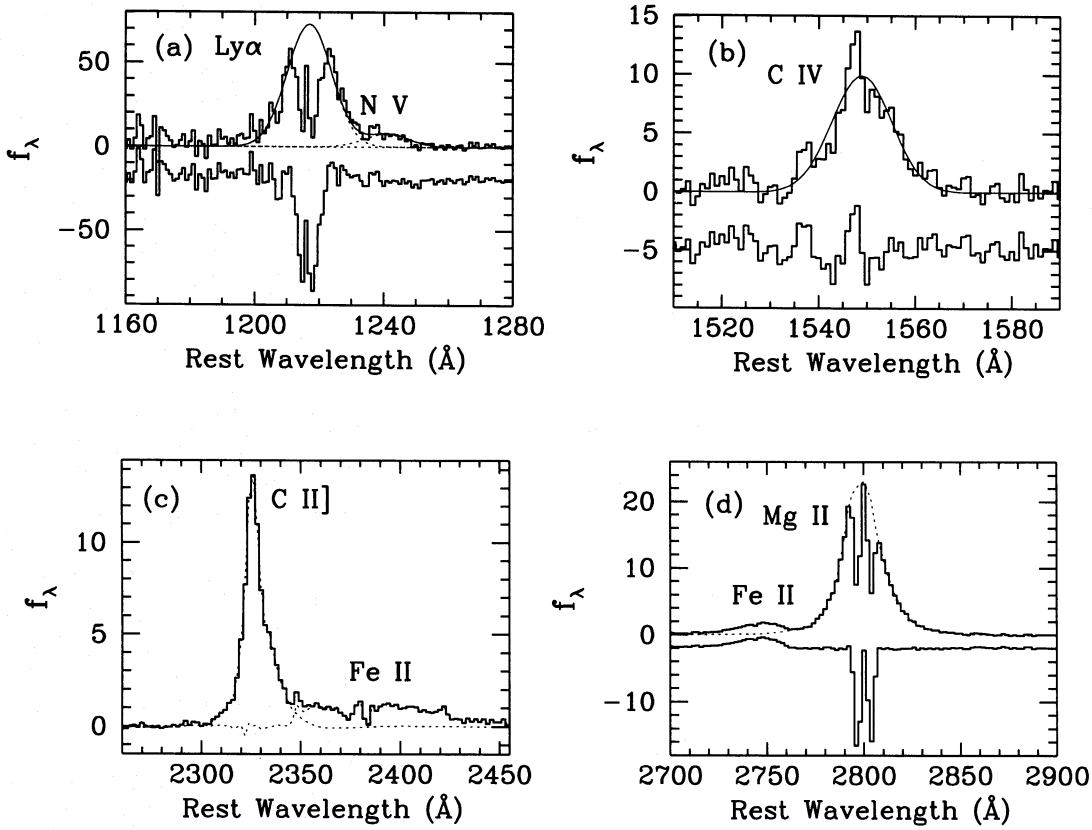

FIG. 5.—Fits to the main UV lines (see text for details). In all cases, the solid histogram displays the data being fitted; the dashed line represents the component(s) of the fit, and, where applicable, the thin solid line shows the best fit derived from summing all individual components. With the exception of (*c*), the solid histogram on the bottom of each panel shows the difference between the data and the model (offset by an arbitrary amount for clarity). (*a*) Two-component Gaussian fit to Lyα and N v λ1240. The "trough" in the center of Lyα is due to interstellar absorption, and the sharp core most likely is geocoronal emission. (*b*) Single Gaussian fit to C II λ1549. (*c*) C II] λ2326 and Fe II complex. A spline function was manually fitted to C II], whose red wing shows substantial asymmetry from its blended multiplets and merges with a shelf of Fe II emission. (*d*) Mg II λ2800 and Fe II complex. Interstellar absorption affects the center of the Mg II line. A spline function was manually fitted to the Mg II line, whose blue wing partly blends with an Fe II complex.

(Fig. 5*b*). Superposed on the underlying broad profile (FWHM = 2800 ± 300 km s^{-1}) is a narrow emission spike blueshifted by 190 km s^{-1} with respect to the centroid of the broad component. The unresolved narrow core, containing ~10% of the flux from the total blend, probably comes from the NLR.

The red half of C II] λ2326, whose apparent asymmetry is due to blending of several multiplets, mergers with an extended shelf of Fe II emission (Fig. 5*c*). To obtain a reasonable decomposition, we resorted to tracing the C II] line manually with a spline function, forcing the blended portion of the red wing to have a continuous shape. Similar to Lyα, Mg II λ2800 has a prominent interstellar absorption component near the center of the line (Fig. 5*d*); its base is clearly non-Gaussian, and the blue wing partly merges with the Fe II complex centered at 2748 Å. As with C II], we traced its emission profile manually with a spline function, assuming that the blue and red wings are roughly symmetric. The resulting Mg II profile has FWHM ≈ 2500 km s^{-1} and wings extending to FWZI ≈ 12,000 km s^{-1}. The superposed absorption renders the profile of the core of the line extremely uncertain, and we cannot determine the narrow-line contribution to the line flux.

Prominent Fe II emission blends are visible at 2380 Å (2345–2430 Å), 2620 Å (2575–2654 Å), 2670 Å (2655–2685 Å), 2748 Å (2725–2760 Å), and 2950 Å (2916–2979 Å). These complexes, which can be identified with UV multiplets (Grandi 1981; Kwan 1984), are usually heavily blended with each other in the spectra of quasars (Francis et al. 1991). Over the region ~2800–3870 Å, the continuum exhibits a hump centered near 3350 Å (Fig. 7). We identify this feature with the so-called small blue bump, comprised mainly of Fe II and Balmer continuum emission (Wills et al. 1985), although in Seyfert 1 nuclei and quasars the bump has a somewhat larger width and peaks near 3000 Å. The offset of the central peak toward longer wavelengths in M81 probably indicates that Fe II contributes less to the total emission than in quasars.

The region between 3800 and 4400 Å is extremely challenging to fit; a multitude of lines are blended, some of which contain both a narrow and broad component. To reduce the number of free parameters, a model narrow-line Balmer series (Hγ–Hζ; Fig. 6*b*), constructed from parameters estimated from the comparatively less complicated [S II] λλ4069, 4076 + Hδ blend, was subtracted from the original spectrum. We fitted the remaining spectrum (Fig. 6*a*) with 10 Gaussians, constrained so that the respective components of the [Ne III] and [S II] doublets have theoretically fixed intensity ratios and wavelength separations, and so that all the broad Balmer lines have identical widths.

The measurement of lines outside of the spectral regions observed with the FOS has been discussed elsewhere (FS; Ho et al. 1993) and will not be repeated here. Table 2 summarizes the results. The errors associated with the entries

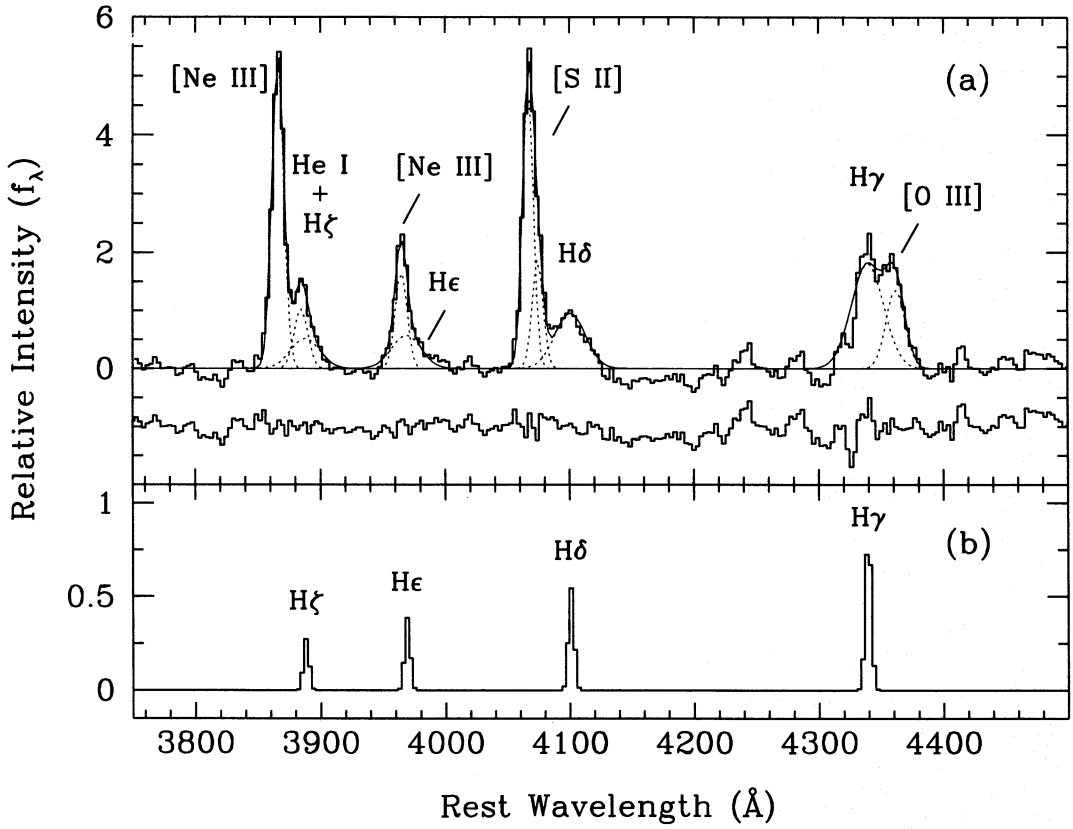

FIG. 6.—Deblending of the 3800–4400 Å section of the G400H spectrum. The labeling convention is the same as in Fig. 5. (*a*) Resulting data after a model spectrum for the narrow component of the Balmer series (*b*) has been subtracted. The relative intensities of the Balmer series are constrained by the reddening adopted for the NLR. The best-fitting model contains a 10-component Gaussian fit to [Ne III] λ3869, He I λ3888, broad Hζ, [Ne III] λ3967, broad Hε, [S II] λλ4069, 4076. broad Hδ, broad Hγ, and [O III] λ4363. Note that the residuals in the range 4150–4300 Å are due to stellar absorption lines and do not reflect the quality of the fit to the emission lines.

represent realistic, conservative estimates of the uncertainties and are *not* formal errors. It is difficult to assess the significance of formal errors (e.g., as obtained from the line-fitting procedure), since the S/N of the FOS data, although much better than that of the ground-based spectra, is still limited, and many constraints had to be imposed to yield meaningful results. Moreover, many lines were subject to nonstandard treatment, as described above, to which formal errors are difficult to assign. Instead, we adopted the strategy of repeating the measurements under a variety of assumptions and then examining the range of acceptable results based on subjective evaluation (e.g., by examining the residuals of the difference between the data and the model).

3.4. *Reddening Estimates*

Based on the ratio of the narrow components of Hα and Hβ, FS concluded that the NLR of M81 is reddened by $E(B-V) = 0.094$ mag (0.038 mag Galactic, 0.056 mag internal). Lacking any additional reliable, independent information, we adopt the same reddening for the portion of the NLR sampled by the much smaller FOS aperture, although this assumes that the reddening is spatially uniform. (In principle, one can obtain a reddening estimate appropriate for the FOS aperture using the narrow component of the Hγ–Hζ Balmer lines in the G400H grating; unfortunately, the weakness of the lines, the relatively low S/N of the data, the complicated deblending procedure, and the small wavelength range do not give a reliable determination of the reddening.)

The reddening for the BLR is difficult to ascertain. As discussed by FS, the physical conditions of the BLR render the ratio of broad Hα to Hβ nearly useless for reddening determination. Based on the ratio of broad Hγ to Hβ, FS argue that the intrinsic reddening of the BLR is ~0.1 mag, with a probable range of 0.0–0.25 mag. While in principle we can make use of the broad components of Hγ–Hζ, they suffer from the same limitations as mentioned for the narrow components.

We can estimate the reddening of the continuum from its shape near the maximum of the extinction curve at 2200 Å, provided that the properties of the dust grains in the nucleus of M81 resemble those of the Galaxy. Although we lack data in the range ~1600–2200 Å, experimentation with the Galactic extinction law of Cardelli, Clayton, & Mathis (1989) showed that the effect of the 2200 Å bump becomes very noticeable for values of $E(B-V) \gtrsim 0.1$ mag and that $E(B-V)$ for the continuum is consistent with 0.0–0.1 mag. If a single power law characterizes the intrinsic shape of the UV continuum, it appears that $E(B-V) = 0.038$ mag yields the most continuous slope in the region between 3000 and 1200 Å (Fig. 7; *bottom solid curve*). A total continuum reddening equal to that deduced for the NLR, on the other hand, introduces slight curvature into the dereddened continuum shape (Fig. 7; *top solid curve*); the departure from a single power law would be even more

TABLE 2

MEASUREMENT OF EMISSION LINES IN M81

Line	Tel.	W_λ	$F(\lambda)/F(H\beta)$	$I(\lambda)/I(H\beta)$	FWHM	FWZI	Notes
(1)	(2)	(3)	(4)	(5)	(6)	(7)	(8)
Lyα λ1216	H	1603±802	15.4±7.7	28.9±14	3970±1000	10000±2000	
N V λ1240	H	165.9±17.4	1.63±0.17	2.97±0.31	3890±350	—	
Si IV+O IV] λ1400	H	65.9±11.9	0.78±0.14	1.22±0.22	—	6200±900	a
N IV] λ1488	H	39.8±8.4	0.53±0.11	0.79±0.17	2800±600	—	b
C IV λ1549 narrow	H	15.96±1.98	0.22±0.03	0.32±0.04	—	—	
C IV λ1549 broad	H	143.6±17.8	1.95±0.24	2.87±0.36	2800±600	8900±2000	
O III] λ1663	I	—	1.03±0.21	1.49±0.29	—	—	c
N III] λ1750	I	—	0.96±0.19	1.37±0.27	—	—	c
Si III] λ1882	I	—	0.48±0.09	0.69±0.13	—	—	c
C III] λ1909	I	83±25	1.83±0.55	2.71±0.81	—	—	c
C II] λ2326	H	164±20	2.41±0.29	3.71±0.45	2200±200	10000±2000	d
Fe II (2344 – 2430)	H	58.8±6.2	0.95±0.10	1.38±0.15	—	—	a
[O II] λ2470	H	27.4±8.5	0.45±0.14	0.62±0.19	900±90	3000±600	
Fe II (2575 – 2654)	H	65.4±7.8	1.10±0.13	1.43±0.17	—	—	a
Fe II (2655 – 2685)	H	10.5±1.2	0.18±0.02	0.23±0.03	—	—	a
Fe II (2725 – 2760)	H	36.6±3.2	0.69±0.06	0.86±0.08	—	—	a
Mg II λ2800	H	456±91	8.74±1.8	10.8±2.2	2530±900	12000±2000	
Fe II (2916 – 2979)	H	6.39±0.49	0.13±0.01	0.16±0.01	—	—	a
O III λ3133	H	1.89±0.13	0.042±0.003	0.049±0.004	—	—	
He II λ3204	H	5.65±0.86	0.13±0.07	0.15±0.07	—	—	
small-bump (2800 – 3870)	H	—	1.68±0.34	1.92±0.39	—	—	a
[Ne V] λ3346	H	4.45±0.41	0.11±0.01	0.13±0.01	1090±300	3300±500	
[Ne V] λ3426	H	8.11±1.2	0.20±0.03	0.23±0.03	1090±300	3300±500	
[O II] λ3727	H	40.6±2.0	1.00±0.05	1.11±0.06	390±20	1210±160	e
[Ne III] λ3869	H	39.4±2.0	0.97±0.05	1.07±0.06	830±170	—	
He I λ3888	H	8.89±0.80	0.22±0.02	0.24±0.02	940±190	—	
Hζ λ3889 narrow	H	0.85±0.17	0.021±0.004	0.023±0.004	260±52	—	
Hζ λ3889 broad	H	9.30±0.80	0.23±0.02	0.25±0.02	2100±400	—	
[Ne III] λ3967	H	12.3±0.79	0.31±0.02	0.34±0.02	830±170	—	
Hε λ3970 narrow	H	1.22±0.23	0.031±0.006	0.034±0.007	260±52	—	
Hε λ3970 broad	H	10.3±1.2	0.26±0.03	0.28±0.03	2100±400	—	
[S II] λ4069	H	30.9±1.6	0.80±0.04	0.86±0.04	700±140	—	
[S II] λ4076	H	12.4±0.77	0.32±0.02	0.35±0.02	750±140	—	
Hδ λ4102 narrow	H	1.87±0.35	0.049±0.009	0.052±0.01	260±52	—	
Hδ λ4102 broad	H	17.2±1.9	0.45±0.05	0.48±0.05	2100±400	—	
Hγ λ4340 narrow	H	3.16±0.61	0.092±0.018	0.097±0.019	260±52	—	
Hγ λ4340 broad	H	30.8±6.2	0.90±0.18	0.95±0.19	2100±400	—	
[O III] λ4363	H	13.2±2.6	0.39±0.078	0.41±0.082	1200±240	—	
[Fe III] λ4658	H	2.08±0.49	0.079±0.019	0.081±0.019	480±95	—	
He II λ4686	H	2.29±0.57	0.089±0.022	0.091±0.022	810±160	—	
Hβ λ4861 narrow	G	—	1.00	1.00	220±45	1050±100	f
Hβ λ4861 broad	G	86±9	2.65±0.27	2.65±0.27	1900±300	4900±1000	f,g
[O III] λ4959	G	—	1.51±0.15	1.49±0.15	360±60	1900±250	f
[O III] λ5007	G	—	4.16±0.42	4.11±0.41	330±60	2580±250	f
[N I] λ5199	G	—	0.20±0.040	0.19±0.040	290	—	e
[N I] λ5200	G	—	0.20±0.040	0.19±0.040	290	—	e
[N II] λ5755	G	—	1.67±0.50	1.58±0.47	810±200	—	
[O I] λ6300	G	—	4.33±0.43	3.99±0.39	370±50	2000±200	f
[O I] λ6364	G	—	1.20±0.12	1.10±0.11	350±50	1600±200	f
[N II] λ6548	G	—	2.60±0.26	2.37±0.24	210±45	1050±100	f
Hα λ6563 narrow	G	—	3.46±0.35	3.15±0.32	210±45	1050±100	f
Hα λ6563 broad	G	445±45	17.5±1.8	15.9±1.6	2200±200	7000±1000	f,g
[N II] λ6583	G	—	7.70±0.77	7.01±0.70	210±45	1050±100	f
He I λ6678	G	—	0.17±0.12	0.15±0.11	300±200	700±500	f
[S II] λ6716	G	—	2.15±0.22	1.95±0.19	190±45	950±100	f
[S II] λ6731	G	—	2.60±0.26	2.35±0.24	210±45	1050±100	f
[O II] λ7319	G	—	2.49±0.55	2.19±0.49	730±180	—	
[O II] λ7330	G	—	1.95±0.43	1.72±0.38	730±180	—	
[S III] λ9532	G	—	2.97±0.89	2.44±0.73	690±150	—	

NOTES ON COLUMNS.—(1) Line identification and rest wavelength; (2) telescope used for observations: H = *HST*, I = *IUE*, and G = ground-based; (3) equivalent width in angstroms measured with respect to the featureless continuum; (4) observed intensity relative to the narrow component of Hβ, for which we adopt a flux of $F(\mathrm{H}\beta) = 5.43 \times 10^{-14}$ ergs s^{-1} cm^{-2}; note that because of the different aperture sizes used for the FOS and ground-based observations, *line fluxes taken with different instruments should not be used for quantitative analyses*; (5) intensity relative to the narrow component of Hβ after dereddening by $E(B-V) = 0.094$ mag; the narrow component of Hβ has a flux of $I(\beta) = 7.44 \times 10^{-14}$ ergs s^{-1} cm^{-2}; (6) FWHM of line in km s^{-1}, corrected for instrumental resolution assuming that the instrumental and intrinsic widths add in quadrature; (7) FWZI of line in km s^{-1}, corrected for instrumental resolution; (8) notes to Table 2: (a) flux obtained by summing between endpoints of the blend; (b) FWHM of Gaussian constrained to be equal to that of C IV λ1549; (c) measured from spectra obtained from the *IUE* archive; these fluxes supersede the earlier values given in Peimbert & Torres-Peimbert 1981 and Ellis et al. 1982; (d) flux obtained by summing entire blend; FWHM and FWZI obtained from the blue half of the main component; (e) FWHM estimated assuming both components of the doublet have equal strength; (f) line fluxes taken from FS; (g) equivalent width obtained by extrapolating the featureless continuum from the FOS measurements.

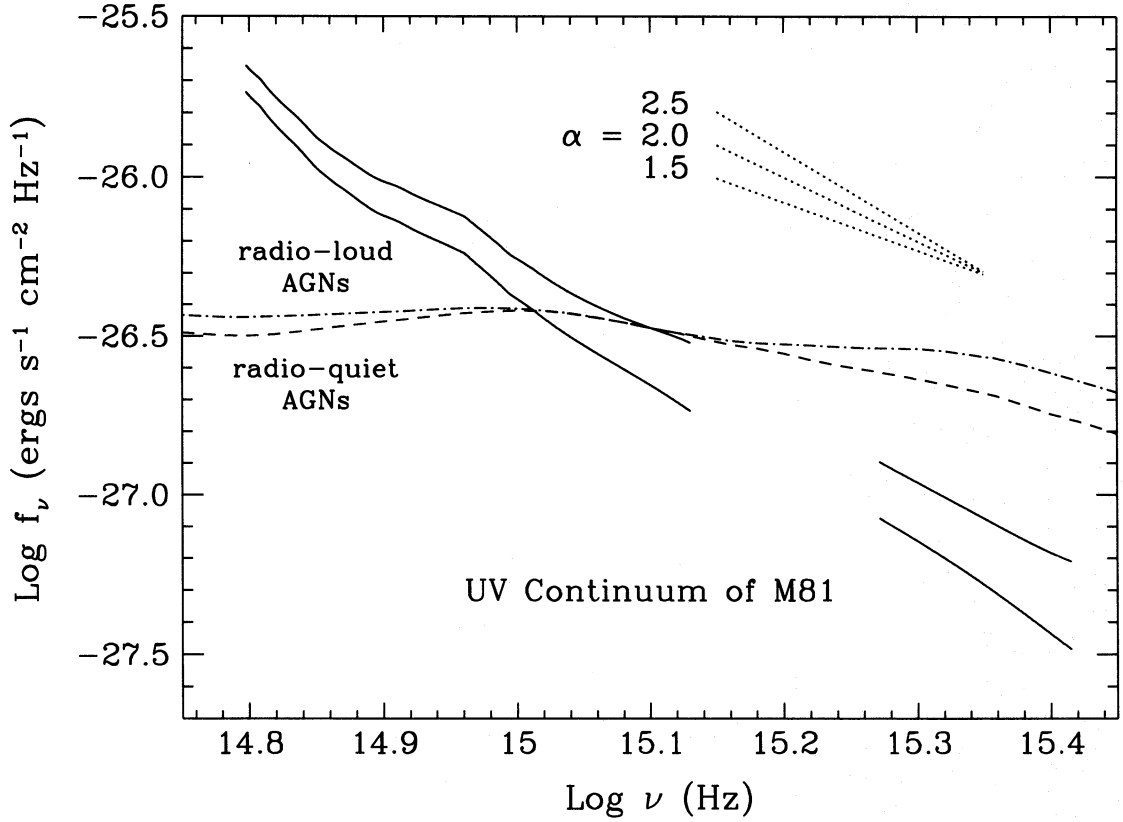

FIG. 7.—Optical-UV featureless continuum of the nucleus of M81 (*solid lines*) shown for two values of $E(B-V)$: 0.038 mag, corresponding to Galactic reddening (*bottom curve*), and 0.094 mag, corresponding to Galactic plus intrinsic NLR reddening (*top curve*). Note the conspicuous "small blue bump" centered near 3350 Å (log $\nu = 14.95$). Power-law functions ($f_\nu \propto \nu^{-\alpha}$) with $\alpha = 1.5$, 2, and 2.5 are shown to guide the eye (*dotted lines*). For comparison, we also show the average continuum shape for radio-loud (*dash-dotted line*) and radio-quiet (*dashed line*) AGNs, both taken from Elvis et al. (1994). The latter two curves were normalized at $\lambda = 2832$ Å (log $\nu = 15.1$) to the flux of M81 for $E(B-V) = 0.094$ mag.

severe if the continuum is reddened by an additional contribution from the BLR. These results may indicate that (1) the Galactic extinction law is inappropriate for the nucleus of M81 (e.g., lacking the 2200 Å bump in M81), (2) the continuum is affected by less reddening than the NLR, or (3) the reddening of the NLR has been overestimated. Without additional constraints, it is unclear which of these explanations is appropriate.

Petre et al. (1993) derived a total hydrogen column density of $(4.1 \pm 1.0) \times 10^{21}$ cm^{-2} from the broad-band X-ray (0.6–10 keV) spectrum of the nucleus; this corresponds to $E(B-V) = 0.69 \pm 0.17$ mag for a Galactic dust-to-gas ratio, much higher than that allowed by the UV continuum shape. If the UV continuum were to be dereddened by this amount, its shape would become highly unusual. Again, the X-ray and UV observations might be reconciled by appealing to differences in the extinction law. It is also conceivable that the dust-to-gas ratio in the nucleus of M81 is lower, or perhaps the region emitting the X-ray continuum is preferentially much more reddened than that emitting the UV continuum. AGNs, especially those of low luminosity, commonly contain higher column densities deduced from soft X-ray observations than from other measures (Mushotzky 1982; Reichert et al. 1985; Turner & Pounds 1989). Guilbert & Rees (1988) argue that cold, X-ray–absorbing material can survive interior to the BLR and to sources of the optical and UV continuum.

For the sake of concreteness, in subsequent discussions we assume that both the BLR and the UV-optical continuum are reddened by the same amount as the NLR [$E(B-V) = 0.094$ mag; note that this differs from the value of 0.138 mag adopted by FS], recognizing that $E(B-V)$ could be as low as 0.038 mag (i.e., zero internal reddening). All the fluxes in Table 2 have been corrected accordingly using the extinction law of Cardelli et al. (1989).

4. DISCUSSION OF RESULTS

4.1. *Detection of the Featureless Continuum*

The difficulty of detecting the ionizing continuum in LINERs has remained one of the main stumbling blocks in resolving the long-standing controversy regarding the excitation mechanism of this class of objects. The intrinsically low luminosity of the central source, coupled with the overwhelming dominance of the stellar background, prohibits measurement of the putative featureless continuum at optical wavelengths except under the most favorable conditions (e.g., NGC 7213, Halpern & Filippenko 1984; M87, Dressler & Richstone 1990). Based on the similarity between several observed properties in Seyfert nuclei and those in a few bright, well-studied LINERs (Filippenko & Halpern 1984; Filippenko 1985; FS), it has been assumed tacitly that a UV nonstellar ionizing continuum must be present, although its presence has not yet been *proved* observationally.

Compared to the optical region, the UV offers the advantage that contamination from the old stellar population is minimized. Although several studies have attempted to use the *IUE* to search for the featureless continuum in LINERs, the results have been largely inconclusive (Bertola et al.

1980; Fosbury et al. 1981; Bruzual, Peimbert, & Torres-Peimbert 1982; Ellis, Gondhalekar, & Efstathiou 1982; Goodrich & Keel 1986; Keel & Windhorst 1991; Reichert et al. 1992a, b, 1993; Kinney et al. 1993). In virtually all cases, the large aperture of *IUE* detected mainly emission from late-type stars, and only crude upper limits could be placed on the presence of a nonstellar continuum. Using optimal extraction techniques, Reichert et al. (1992a, b, 1993) were occasionally able to separate the nuclear emission from the more extended galaxy background, but the PSF (FWHM $\approx 1''$–$2''$) still encircled sufficient starlight to obfuscate the results. To our knowledge, the only reported detection of a featureless UV continuum in a LINER is that of Kollatschny & Fricke (1984) for Mrk 266A. Within the limitations of the low S/N *IUE* data, both nuclei of Mrk 266 (A = LINER, B = Seyfert 2; Mazzarella & Boroson 1993) show an apparently featureless, power-law continuum with a spectral index of $\alpha = 2.0 \pm 0.5$ ($f_\nu \propto \nu^{-\alpha}$).

The present study provides an unambiguous detection of the featureless UV continuum in the nucleus of M81. Although the exact shape of the continuum depends on the assumed value of the reddening (Fig. 7), for $E(B-V) = 0.094$ mag the continuum in the regions covered by the G270H and G130H gratings can be reasonably represented by a power-law function with $\alpha = 2.0 \pm 0.3$, where the uncertainty denotes the range of possible slopes between 3000 and 1200 Å. The steepening of the continuum in the G400H spectrum ($\Delta\alpha \approx 1$) most likely is due to contamination by starlight, although the contribution from the underlying power-law component is still substantial (§ 3.1.5). As discussed in § 3.3, the broad excess centered near 3350 Å can be attributed to the small blue bump. The featureless continuum in M81 is extremely faint: extrapolating the power-law component from shorter wavelengths, $M_B = -11.6$ mag, only a factor of 5 more luminous than that of the least luminous Seyfert 1 nucleus known (NGC 4395; Filippenko & Sargent 1989). The phenomenal weakness of these nuclei provides a stark contrast to conventionally studied Seyfert 1 nuclei characterized by -23 mag $\lesssim M_B \lesssim -16$ mag (Weedman 1976).

Comparison of the M81 continuum shape with the average one for luminous AGNs (Elvis et al. 1994) reveals some striking differences (Fig. 7). If we regard the region blueward of the small blue bump ($\lesssim$3000 Å) as representing the true nuclear continuum, its slope is significantly steeper than that observed in luminous AGNs ($\alpha \approx 0.5$–1; Malkan 1988). Another difference is the conspicuous absence of the "big blue bump" in M81, a feature commonly found in luminous AGNs and traditionally attributed to thermal radiation from an accretion disk (Malkan & Sargent 1982; but see Barvainis 1993 and references therein).

The shape of the featureless continuum can provide important constraints on the physical nature of the central source. Before rushing to the immediate conclusion that the UV continuum has a nonstellar origin, it is worthwhile to consider if hot stars alone can produce the same power-law shape. This is an important consideration for theories that postulate that most AGNs, especially those of lower luminosity, derive their power from stellar activity (Terlevich et al. 1992 and references therein). Several authors, in fact, have advanced specific stellar models to explain the excitation of LINERs (see Shields 1994 for review). We consider two possibilities for M81: (1) a population of evolved, hot stars, such as that responsible for the so-called UV upturn in elliptical galaxies (Burstein et al. 1988; Ferguson & Davidsen 1993), and (2) young, massive stars.

As discussed at length by Ferguson & Davidsen (1993), several types of hot, evolved stars contribute to the excess far-UV flux observed in the centers of many elliptical galaxies and spiral bulges. In such systems, the integrated spectrum for $\lambda \lesssim 1500$ Å can be very blue, with the degree of UV excess being positively correlated with the metallicity (Burstein et al. 1988). However, the UV continuum of M81 does not resemble that of M31 for $\lambda \lesssim 1600$ Å (Ferguson & Davidsen 1993); the continuum slope of M81 is much steeper. Moreover, galaxies with strong UV upturns have much redder continua for $\lambda \gtrsim 1600$ Å. As a concrete example, we examine the FOS spectrum of NGC 3610 (kindly provided by H. C. Ferguson in advance of publication), an E5 galaxy with a UV upturn. The following spectral indices were measured: α(1600—2200 Å) = 8.8 and α(2400–3200 Å) = 9.2. In addition, prominent absorption features due to F and G dwarfs dominate the continuum at 2650, 2850, and 3050 Å, whereas none of these features are detected in M81. From this comparison, we conclude that stars responsible for the UV upturn in elliptical galaxies cannot be a strong contributor to the UV emission in the central 2–3 pc of M81.

Young, massive stars from recent star formation, on the other hand, *could* mimic the overall blueness of the featureless continuum without necessarily violating the absence of stellar absorption lines, although we note that most of the UV spectral energy distributions of the star-forming galaxies in the sample of Storchi-Bergmann, Kinney, & Challis (1995) are in fact flatter than that of M81. O-type stars produce conspicuous absorption or P Cygni lines of S IV and C IV, but these may be filled in by nebular emission. Thus, the absence of these lines alone cannot be used as evidence against the presence of young stars. In cooler stars, one might find Si II + Si III λ1302, C II λ1335, and Si II λ1260 absorption, but, unfortunately, these features can be confused with interstellar absorption. What *does* constitute powerful evidence against a stellar origin for the continuum is the decisively nonthermal nature of the X-ray emission. Besides the nonthermal shape of the X-ray continuum, X-ray emission features observed in prototypical starburst systems are virtually absent in M81 (Petre et al. 1993). Unless the featureless UV continuum and the X-ray emission arise from totally separate components, an energetically important contribution from young stars can probably be ruled out.

4.2. *Spectral Energy Distribution*

In view of the detection of the nonstellar UV continuum and the recently reported broad-band X-ray measurements (Petre et al. 1993), a reexamination of the spectral energy distribution of the nucleus of M81 may shed new insight into its physical nature. To this end, we assembled continuum measurements from a number of sources to construct the broad-band radio to X-ray energy spectrum (Fig. 8).

Whenever possible, we selected measurements made with the smallest aperture available so as to isolate the nuclear component. In the radio regime, we chose the VLBI measurements of Bartel et al. (1982) and the fairly high-resolution ($1''$) VLA maps of Bash & Kaufman (1986) and Turner & Ho (1994). Although variability of at least a factor of 2 has been observed at 2.7 GHz (Crane, Giuffrida, & Carlson 1976), the spectral index between 2.7 and 8 GHz

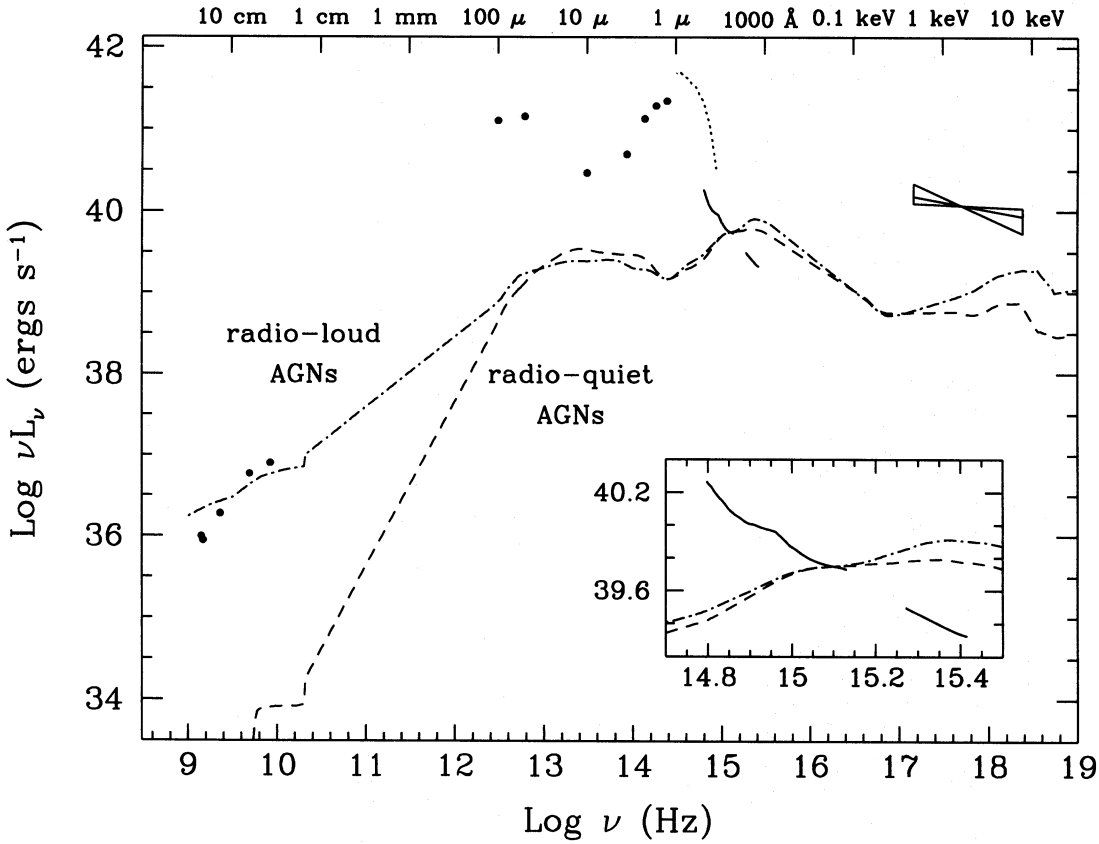

FIG. 8.—Spectral energy distribution of the nucleus of M81. The ordinate shows log νL_ν (ergs s^{-1}), the bottom abscissa log ν (Hz), and the top abscissa some fiducial wavelengths. The data points were taken from the following sources: 1.41 GHz from Bash & Kaufman (1986); 1.49 and 4.89 GHz from Turner & Ho (1994); 2.3 and 8.3 GHz from Bartel et al. (1982); 50 and 100 μm from Rickard & Harvey (1984); 10 μm from Rieke & Lebofsky (1978); L (3.5 μm) from Willner et al. (1985); J (1.25 μm), H (1.65 μm), and K (2.2 μm) from Forbes et al. (1992); optical (3500–9800 Å, *dotted line*) from this work; UV (2230–4770 Å and 1200–1600 Å) from this work, assuming $E(B-V) = 0.094$ mag; and 0.6–10 keV from Petre et al. (1993). The "bow-tie" shape of the X-ray data represents $\pm 1\ \sigma$ error bars for the spectral index between 0.6 and 10 keV. Also plotted are the mean spectral energy distributions for radio-loud (*dot-dashed line*) and radio-quiet (*dashed line*) AGNs (Elvis et al. 1994), normalized to the flux of M81 at $\lambda = 2382$ Å. The inset at the lower right in the figure shows an expanded view of the UV region.

does not vary much (de Bruyn et al. 1976). The far-IR (50 and 100 μm) data points were obtained with the Kuiper Airborne Observatory with a beam of $\sim 50''$ (Rickard & Harvey 1984); consequently, a large fraction of the emission must come from the surrounding galaxy. Using a PSF fitting technique, Forbes et al. (1992) derived a "nuclear" flux in the K band (2.2 μm) that contained 59% of the total flux in a 3″ measurement aperture. Since Forbes et al. did not perform the same analysis for the J (1.25 μm) and H (1.65 μm) images, we assumed that the nuclear component contains the same fraction of light in these two bands. The L-band (3.5 μm) was obtained from the 5″ beam data of Willner et al. (1985) after scaling it down by a factor determined from the ratio of the 5″ to 3″ K-band fluxes (Forbes et al. 1992), while the N-band (10 μm) data were taken directly from Rieke & Lebofsky (1978; 3.″9 aperture). The optical continuum points (3500–9800 Å) were derived from the Palomar spectrum taken on 1990 February 10 UT, and the FOS continuum of Figure 7 [assuming $E(B-V) = 0.094$ mag] is reproduced. Finally, we show the best-fitting broad-band (0.6–10 keV) X-ray spectrum of Petre et al. (1993); we only include the power-law ($\alpha_x = 1.20^{+0.3}_{-0.15}$) component of the spectrum, since the softer, coronal plasma ($kT = 0.4$ keV) component presumably arises exterior to the nucleus (Petre et al. 1993). For comparison, we have also plotted the mean spectral energy distribution of radio-loud and radio-quiet AGNs (Elvis et al. 1994), normalized to M81 at $\lambda = 2382$ Å ($\nu = 10^{15.1}$ Hz), as in Figure 7.

Several salient features are immediately apparent. (1) With the exception of the radio, UV, X-ray, and possibly 10 μm measurements, all of the remaining data points are heavily contaminated by galactic emission. This is hardly surprising for the optical and near-IR bands, where the continuum in M81 and other LINERs is known to be dominated by evolved stars (Ho et al. 1993; Forbes et al. 1992). Similarly, the coarse aperture of the far-IR measurements is expected to include mainly emission from warm dust. However, despite the relatively large aperture (3.″9) used for the measurement, the 10 μm continuum probably contains mostly nuclear emission. There is some observational support that at this wavelength the nuclei of LINERs tend to be brighter than those of normal spirals, and that the excess emission arises from thermal emission of dust heated by a central source (Lawrence et al. 1985; Willner et al. 1985). (2) If we normalize the continuum points to those of normal AGNs in the UV, the nucleus of M81 technically can be considered "radio-loud," although if we had chosen the normalization in the X-rays, the radio power would have been intermediate between "radio-loud" and "radio-quiet." (3) The shape of the UV continuum of M81 is much steeper than that of luminous AGNs, and the big blue bump is absent (§ 4.1). Unlike the case in normal AGNs, the UV

continuum of M81 contributes minimally to the bolometric luminosity. Indeed, the spectral energy distribution continues to decrease even at the shortest UV wavelength measured (~1150 Å). (4) As discussed by Petre et al. (1993), the X-ray spectrum is much steeper than that of luminous AGNs. (5) The nucleus of M81 is very bright in X-rays relative to UV radiation. The two-point spectral index between 2500 Å and 2 keV, α_{ox}, is 0.86, significantly smaller than the average for quasars (1.4) or Seyfert 1 nuclei (1.2) given in Mushotzky & Wandel (1989). In fact, the 0.6–10 keV region accounts for nearly 75% of the bolometric luminosity ($2.4 \times 10^7\ L_\odot$; § 4.4), whereas only ~10% comes from the region between 912 Å and 0.6 keV. It should be noted that the X-ray flux of the nucleus of M81 shows variability over long timescales. Had we chosen the measurement taken when the X-ray flux of M81 was in its historically lowest state (§ 4.5), the spectral energy distribution of the nucleus would look quite different (Fabbiano 1996); however, the nucleus has been in its X-ray–bright state for the past several years (Petre et al. 1993).

4.3. *Kinematics and Physical Conditions of the Line-emitting Gas*

4.3.1. *The Narrow-Line Region*

FS demonstrated that the forbidden lines in the nucleus of M81 obey the correlation between line width and critical density previously established in some LINERs (Filippenko & Halpern 1984; Filippenko 1985) and Seyfert 2 nuclei (De Robertis & Osterbrock 1986), and that the correlation is more significant than that between line width and ionization potential. Since the present study includes a much larger set of emission lines, we wish to reevaluate the line width correlations.

Our results confirm and strengthen the findings of FS. As shown in Figure 9*a*, the widths (FWHM) of the forbidden lines show a remarkable correlation with the critical densities (n_{crit}), with both variables spanning a large dynamic range.[4] Transitions arising from the same ion (and hence having the same ionization potential [χ]) but having different values of n_{crit} show different line widths. This point is clearly illustrated by comparing the following pairs of lines (Table 2): [S II] λλ6716, 6731; [S II] λλ4069, 6731; [O II] λλ3727, 7325; [N II] λλ5755, 6583; and [O III] λλ4363, 5007. A weighted, linear least-squares fit to all the lines yields a slope (m) of 0.11 ± 0.010 with a Spearman rank correlation coefficient (r_S) of 0.89; the probability (P) that the data points could have been drawn from a random distribution is 5.5×10^{-6}. Closer examination reveals that the lines with low n_{crit} ([N I], [O II] λ3727, and [S II] λλ6716, 6731) appear to deviate systematically from the tighter correlation formed among the lines with higher n_{crit} (Fig. 9*a*, *dashed line*). Considering only the lines with $n_{crit} \gtrsim 10^4$ cm^{-3}, the correlation is still highly significant ($r_S = 0.89$ and $P = 1.8 \times 10^{-4}$), and the slope increases to $m = 0.31 \pm 0.037$, much closer to the theoretically predicted value of 0.25 (FS). (We note that [S III] λ9532 deviates appreciably from the best-fitting line. As remarked in Ho et al. 1993, some of the atomic parameters of S^{++} may be uncertain.)

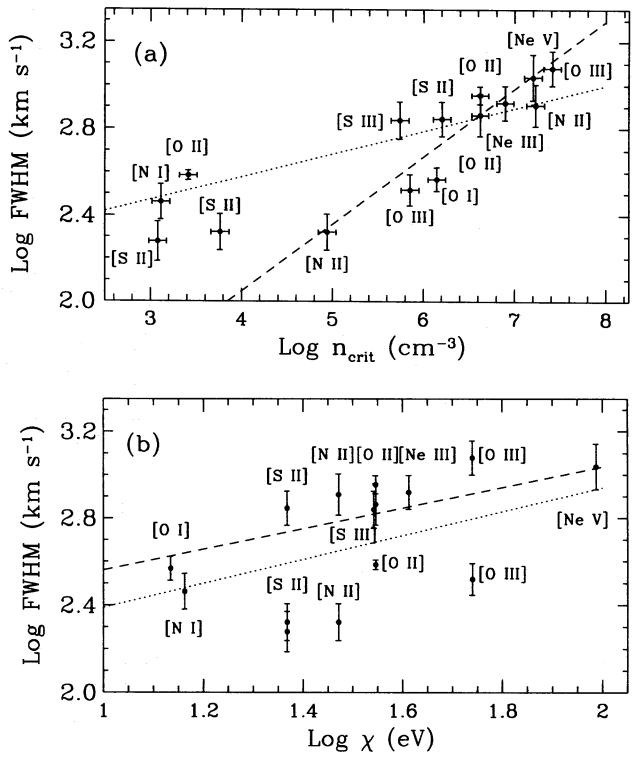

FIG. 9.—Correlations between the FWHM and (*a*) the critical density (n_{crit}) and (*b*) ionization potential (χ) of the forbidden lines in M81. The FWHM measurements have been corrected for instrumental resolution. We calculated the values of n_{crit} for each transition using atomic parameters given in Osterbrock (1989), and errors of ±25% have been assumed. In each panel, the weighted linear least-squares fit to the data is shown for all data points (*dotted line*) and excluding the low-density transitions [O II] λ3727, [N I] λ5200, and [S II] λλ6716, 6731 (*dashed line*). In (*a*) the slopes for the two fits are, respectively, $m = 0.11 \pm 0.010$ and 0.31 ± 0.037, and the Spearman rank correlation coefficients (r_S) are 0.89 and 0.89, with the probability (P) that the correlations are random, being 5.5×10^{-6} and 1.8×10^{-4}, respectively. In (*b*) the corresponding values are $m = 0.55 \pm 0.092$ and 0.48 ± 0.11, $r_S = 0.65$ and 0.55, and $P = 8.9 \times 10^{-3}$ and 8.0×10^{-2}.

By contrast, the correlation between FWHM and χ is much weaker (Fig. 9*b*), although it can still be regarded as significant, probably because most lines having high n_{crit} also have high χ. For the two cases considered (i.e., including and excluding the low n_{crit} lines), $m = 0.55 \pm 0.092$ and 0.48 ± 0.11, $r_S = 0.65$ and 0.55, and $P = 8.9 \times 10^{-3}$ and 8.0×10^{-2}, respectively.

The FWHM versus n_{crit} correlation provides compelling evidence that the NLR in M81 is stratified strongly in density. As suggested by FS, it appears that the structure of the NLR is composed of two distinct components: a low-density (n = a few times 10^2–10^3 cm^{-3}) reservoir or "halo" located at large separation from the continuum source, primarily emitting lines of low n_{crit}, and a more compact, intermediate- to high-density ($n = 10^4$–10^7 cm^{-3}) core, wherein lines of high n_{crit} dominate. The core component itself is strongly stratified in density, giving rise to the observed FWHM versus n_{crit} correlation. The density of the "halo" can be estimated directly from the ratio of [S II] λ6716 to [S II] λ6731, whose critical densities are 1.2×10^3

[4] In the following discussion, we will not be concerned with the effect of the aperture size on line widths. The widths of lines detected in common in the *HST* and ground-based spectra are nearly identical within observational errors. In view of the sizes predicted for the various emitting regions (see below), lines with critical densities $\gtrsim 10^4$ cm^{-3} should be unresolved with a 0.″3 aperture, and, hence, both the *HST* and ground-based measurements sample the same regions for these lines. The low-density lines ([O II] λ3727, [N I] λ5200, and [S II] λλ6716, 6731), although resolved by *HST*, should be largely contained within the slit of the ground-based observations; thus, in the analysis of the line widths for these three lines, we use the measurements from the ground-based spectra.

cm^{-3} and 5.8×10^3 cm^{-3}, respectively. The observed ratio of 0.83 corresponds to an electron density (n_e) of ~ 900 cm^{-3} for an electron temperature of 10^4 K (J. Halpern and A. Filippenko, unpublished calculations). The ratio [O II] λ7325/Hα, on the other hand, implies $n \gtrsim 10^6$ cm^{-3} (see Fig. 7 in Ho et al. 1993), consistent with $n_{crit} = 4.2 \times 10^6$ cm^{-3} for [O II] λ7325.

As discussed in detail by FS and Filippenko & Halpern (1984), a correlation of the form FWHM $\propto n_{crit}^m$, with $m = 0.25$, is anticipated if (1) the velocities as measured by the line widths are due to Keplerian rotation, (2) each forbidden line preferentially emits from gas with $n \approx n_{crit}$, and (3) the ionization parameter ($U \equiv$ ratio of ionizing photon density to gas density at the illuminated face of the cloud) within the NLR remains approximately constant with radius (or, equivalently, $n \propto r^{-2}$). Although the observed value of $m = 0.31$ is consistent with this picture, one must not be complacent about the validity of all of the above assumptions. Indeed, the more detailed treatment of the structure of the NLR in Seyfert 2 nuclei by Whittle (1985) cannot account for the large range in line widths observed in M81 and other LINERs. Kinematic models reflecting the physical conditions in LINERs need to be explored to address this issue. Moreover, it would be highly desirable to obtain high-dispersion echelle spectra to study in detail the profiles of the narrow lines. The distinctly non-Gaussian shapes of the narrow lines of M81 (FS) suggest that the profiles contain multiple velocity components. The higher resolution observations of Keel (1989), for example, reveal that both [N I] λ5200 and [O III] λ5077 have a broader wing, in addition to a narrow core. These and additional high-resolution data for a large number of transitions need to be incorporated into more sophisticated models of the NLR.

In some Seyfert nuclei, although certainly not all (Whittle 1985; De Robertis & Shaw 1990), lines of high χ preferentially have higher radial velocities. We find no such trend in M81.

The measured ratio of [O III] $\lambda\lambda$4959, 5007/λ4363 = 13.7 gives an electron temperature for the O^{++} region of 15,000 and 8000 K for $n_e = 10^6$ and 10^7 cm^{-3}, respectively, consistent with temperatures expected for photoionized nebulae. An independent estimate of T_e can be obtained for the N^+ region: for $n_e = 10^6$ cm^{-3}, the observed ratio [N II] $\lambda\lambda$6548, 6583/λ5755 = 5.9 yields $T_e \approx 8000$ K. It is possible that the actual electron densities are somewhat smaller than those assumed here, in which case the derived electron temperatures would be higher and more compatible with those of shock-heated plasmas. The predictions of recent autoionizing shock models (Dopita & Sutherland 1996) should be compared with the spectrum of M81.

The intensity ratios of several narrow optical lines are sensitive to U. These include [O II] λ3727/[O III] λ5007, [O III] λ5007/Hβ, and [Ne V] λ3426/[Ne III] λ3869. Using the first two of these, we estimate from the photoionization models of Ho et al. (1993 and unpublished calculations) that $\log U \approx -3.3$; however, the relatively high ratio of [Ne V] λ3426/[Ne III] λ3869 = 0.2 requires an additional component with $\log U \approx -2.3$. The presence of more than one ionization-parameter component in the NLR obviously conflicts with one of the assumptions in our simple density-stratification picture and indicates that the actual NLR structure must be more complicated.

Having obtained estimates of U and n, we can calculate the typical sizes of the emitting regions with knowledge of the total ionizing luminosity. Assuming spherical symmetry and a uniform covering factor, the distance between an illuminated cloud and the central ionizing source is $r = (Q_H/4\pi cnU)^{1/2}$, where Q_H is the total number of ionizing photons s^{-1}. For a power-law ionizing continuum [$L_\nu = L_0(\nu/\nu_0)^{-\alpha}$ ergs s^{-1} Hz^{-1}], $Q_H = (L_0 \nu_0^\alpha/h\alpha)(\nu_0^{-\alpha} - \nu_{max}^{-\alpha})$ s^{-1}, where h is Planck's constant, and ν_0 (the Lyman limit) and ν_{max} specify the limits of the integration. We assume that the unobserved region between 912 Å and 0.6 keV (§ 4.2) can be approximated by a single power law connecting the two points, and that the X-ray spectral slope ($\alpha_x = 1.20^{+0.3}_{-0.15}$; Petre et al. 1993) remains constant to 200 keV. We obtain the luminosity at the Lyman limit by extrapolating a power law with $\alpha = 2.0$, with L_0 normalized at $\lambda = 1200$ Å. For the observed range of α_x, we find $Q_H = (1.0\text{–}1.2) \times 10^{50}$ s^{-1}. Assuming $\log U = -3.3$ in the NLR, $n = 10^3$, 10^4, and 10^5 cm^{-3} correspond to $r_{NLR} = 7.4$, 2.3, and 0.7 pc, respectively. Since some of the emission-line regions seem to have higher values of U, these size estimates should be regarded as upper limits.

Compared with the majority of LINERs (see Ho et al. 1993), M81 exhibits among the strongest [O I], [S II], and [N II] lines. However, with the possible exception of N, which might be enhanced by a factor of ~ 1.5 relative to solar abundance, it is unnecessary to invoke selective enrichment of O and S to explain the strengths of these lines. The hardness of the ionizing continuum in M81 (§ 4.2) is expected to create in the line-emitting clouds rather extensive partially ionized zones, where most of the low-ionization lines radiate.

Given the considerable complexity of the density structure of the NLR, the above comparisons with single-zoned calculations are only meant to be illustrative. Multizoned models, taking into account the observed spectral energy distribution, need to be evaluated in the future.

4.3.2. *The Broad-Line Region*

The broad lines detected in M81 show a range of line widths (Fig. 10). The broad UV permitted lines and Hα have roughly comparable widths (FWHM; see Table 2). Lyα has a larger FWHM, but its value is heavily influenced by our assumption of the intrinsic, unabsorbed profile (Fig. 5*a*), which is highly uncertain. Despite the considerable difficulty in defining the extent of the wings of the lines, especially for Lyα and C IV, it is obvious that the FWZIs of the UV lines are larger than that of Hα. Mg II λ2800, in particular has FWZI $\approx$ 12,000 km s^{-1}. Detailed models of the BLR (e.g., Ferland et al. 1992) find that Lyα (and perhaps C IV for high U) should be emitted anisotropically. The apparent lack of significant asymmetry in the Lyα and C IV profiles of M81 rules out radial motions as a major component of the velocity field in its BLR.

Prior to the present study, the existence of BLRs in LINERs has been inferred almost exclusively from the detection of the broad Hα emission line (Filippenko & Sargent 1985). With the exception of previous *IUE* studies of M81 (Peimbert & Torres-Peimbert 1981; Reichert et al. 1993), the only broad UV line detected unambiguously has been Mg II λ2800 (NGC 4579, Reichert, Puchnarewicz, & Mason 1990; NGC 3998, Reichert et al. 1992a). In the case of M81, the data presented by Reichert et al. (1993) did not have sufficient S/N to detect the full extent of the broad wings of the UV emission lines. The *IUE* data also lacked

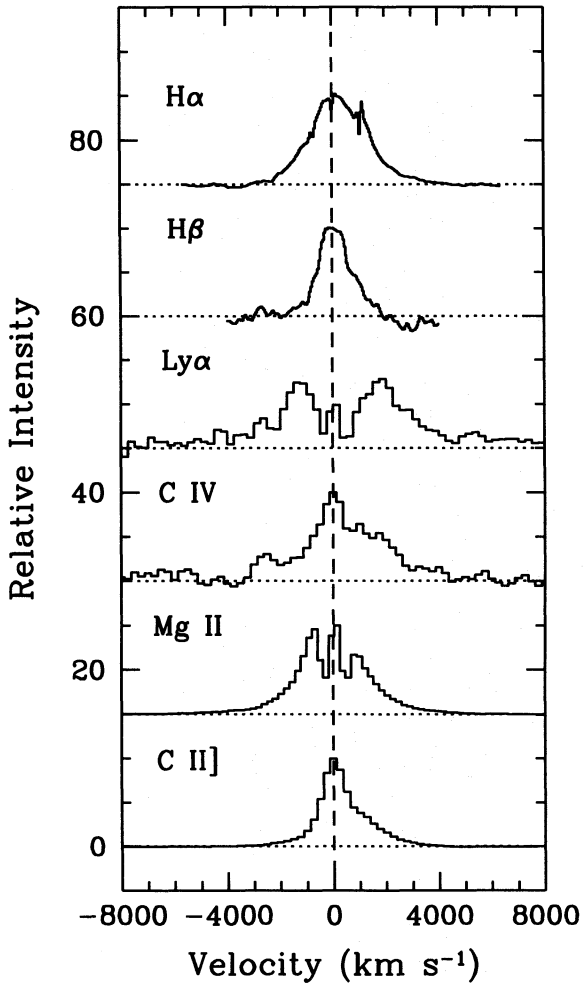

FIG. 10.—Profiles of broad permitted lines and of C II] λ2326. The ordinate plots relative intensity in arbitrary units, and the abscissa velocity in km s^{-1}. Each line is normalized to the same peak intensity, and each successive line is displayed by 15 units in the ordinate for clarity. For Hα, Hβ, and C IV, the peak of the narrow component was used to center the velocity scale, while for C II] the centroid of the main transition was used. Lyα and Mg II were arbitrarily shifted to approximately center the broad wings. Note that the asymmetry on the red side of C II] is due to a blend of several C II] transitions.

the spectral resolution to discern the Mg II absorption, leading Reichert et al. to conclude that the core of the Mg II emission line was abnormally suppressed. Given such limited information, not much could be deduced about the physical conditions of the BLR in LINERs.

The conventional practice in estimating U and n for the BLR once again makes use of photoionization models to match certain diagnostic line ratios. As shown by Mushotzky & Ferland (1984), for instance, the ratio C IV λ1549/Lyα is a sensitive indicator of U, while C III] λ1909/C IV measures n. This simple method, however, idealizes the BLR as a single-zone cloud, an assumption that no longer seems tenable in view of recent developments (see, e.g., Peterson 1993). Variability studies of several Seyfert 1 nuclei clearly show that the BLR, at least in the few objects monitored intensively, has a stratified ionization structure. Specifically, unlike C IV and Lyα, which seem to be roughly cospatial, C III] is emitted predominantly at a much larger radius from the central source, rendering the C III]/C IV ratio useless as a density indicator unless very detailed variability information is available (e.g., Krolik et al. 1991; Ferland et al. 1992). For the well-studied case of NGC 5548, Ferland et al. (1992) estimated a density for the Lyα–C IV zone that is at least a factor of 10 higher than would have been obtained using the conventional method.

M81, unfortunately, does not appear to vary in its broad Hα emission (§ 4.5), and nothing is known about the variability characteristics of other lines or of the continuum at any wavelength other than the radio. Conceivably, the BLR structure of LINERs and low-luminosity Seyferts, for reasons not yet understood, may differ from that of more luminous sources. Thus, it is unclear how the results based on recent variability studies apply to low-luminosity sources (or, for that matter, to any other AGNs with variability properties differing substantially from those of the Seyfert 1 nuclei targeted; Peterson 1993). Lacking any alternative, we will estimate U and n in the traditional fashion, bearing in mind that the density could be severely underestimated. From the observed value of C IV/Lyα ≈ 0.1, we find $\log U \lesssim -2.8$ (Kwan 1984; Mushotzky & Ferland 1984); this is an upper limit because the flux of Lyα most likely is a lower limit (§ 3.3). The observed ratio N V λ1240/Lyα ≈ 0.1, on the other hand, gives a much higher value ($\log U \lesssim -1.4$). This apparent inconsistency is not uncommon in luminous AGNs (Kwan 1984), and it may indicate the presence of a high-U component in the BLR. Mushotzky & Ferland (1984) find that Seyfert 1 nuclei and QSOs show a weak, but nevertheless significant, inverse correlation between U (derived from C IV/Lyα) and L_{1450}, the luminosity of the continuum at $\lambda = 1450$ Å. They find, for example, that the BLRs of QSOs and Seyfert 1 nuclei typically have $\log U \approx -2.5$ and -1.5, respectively. M81 ($L_{1450} = 1.6 \times 10^{24}$ ergs s^{-1} Hz^{-1}) does *not* follow this correlation.

Assuming $\log U \approx -2.8$, the observed ratio C III]/C IV ≈ 0.9 indicates $n \lesssim 10^9$ cm^{-3}. We also estimated n using several other line ratios suggested by Kwan (1984). The ratios of Si IV + O IV] λ1400, N IV] λ1488, and O III] λ1663 to C III] (0.4, 0.3, and 0.6, respectively), as well as Balmer continuum to Hβ (0.7; we assume that Fe II emission is a small contributor to the small blue bump [§ 3.3]), all give $n \approx 10^9$ cm^{-3}. The profile of C II] λ2326 provides an additional important constraint (Fig. 10). Contrary to the *IUE* results of Reichert et al. (1992b), we find that both the FWHM (~2200 km s^{-1}) and FWZI (~8000–12,000 km s^{-1}) of C II] are comparable to those of Mg II λ2800. (The FWZI is uncertain because of probable contamination by Fe II emission in the blue wing of C II].) Since both C II] and Mg II originate roughly from the same region of the BLR (Kwan & Krolik 1981), we conclude that in the Mg^+ zone $n \lesssim n_{crit}(\text{C II}]) \approx 2 \times 10^9$ cm^{-3}, consistent with the other determinations. Finally, the lack of broad [O III] λλ4959, 5007 emission sets a lower limit of $n = 10^7$ cm^{-3}, above which these lines become severely collisionally de-excited. [O III] λ4363, with a higher critical density, can in principle set a higher lower limit, but a broad component would be difficult to discern in such a weak line.

The relative intensity ratios of the entire broad-line spectrum of M81 roughly agree with the model predictions for $U \approx 10^{-2.8}$ and $n \approx 10^9$ cm^{-3}. The large ratio Mg II/Hβ ≈ 4, for instance, is to be expected for the low value of U. Under these conditions, the models of Mushotzky & Ferland (1984) predict that He II λ4686/C IV ≈ 0.04. Assuming that He II λ1640/λ4686 = 6–8 (Seaton 1978), we

expect that He II λ1640/C IV ≈ 0.3, in excellent agreement with observations (Reichert et al. 1992b).[5]

The low value of U deduced from the C IV/Lyα ratio in the BLR of M81 may be a general property of most or all LINERs having weak, broad emission lines. Keel & Windhorst (1991) detected Lyα and C IV in four LINERs using *IUE*; in all cases, C IV/Ly$\alpha \lesssim 0.1$. Mrk 266A also has very low C IV/Lyα (0.05; Kollatschny & Fricke 1984). Likewise, most LINERs with detected C III] and C IV indicate relatively low n in their BLRs: C III]/C IV $\gtrsim 1$ in NGC 3998, ≈ 1 in NGC 4579 (Reichert et al. 1993), and $\gtrsim 1$ in NGC 1052 (Fosbury et al. 1981). NGC 7213 (Filippenko & Halpern 1984) and Mrk 266A (Kollatschny & Fricke 1984) have somewhat lower C III]/C IV.

Assuming that $U = 10^{-2.8}$ and $n = 10^9$ cm^{-3} crudely describes the BLR, $r_{\rm BLR} = 0.004$ pc. If n has been underestimated by a factor of 10, $r_{\rm BLR} = 0.001$ pc. These dimensions are roughly consistent with the radius-luminosity relation ($r_{\rm BLR} \propto L^{1/2}$) obeyed by Seyfert nuclei (Peterson 1993). For instance, if one were to derive the size of the BLR of NGC 5548 in an analogous fashion, $r_{\rm BLR} \approx 0.1$ pc (Peterson 1993), in approximate agreement with the above scaling relation because its ionizing luminosity ($Q_{\rm H} \approx 10^{54}$ s^{-1}; Peterson 1993) is 10^4 times greater than that of M81.

4.3.3. *Energy Budget*

The general consistency between the observed emission-line spectrum and the predictions of conventional BLR models suggests that photoionization by a nonstellar continuum provides most of the excitation for the gas.

We further check this conclusion by comparing the observed broad Hα luminosity with the X-ray luminosity. In luminous AGNs, these two quantities show a strong correlation over an enormous range in luminosity (e.g., Kriss, Canizares, & Ricker 1980; Elvis, Soltan, & Keel 1984), from which it has been argued that all AGNs must be powered by photoionization. Petre et al. (1993) found that the power-law component of the X-ray luminosity between 2 and 10 keV is $(1.8 \pm 0.4) \times 10^{40}$ ergs s^{-1}. Combining this with our broad Hα luminosity of 1.8×10^{39} ergs s^{-1} (dereddened), we obtain L(2–10 keV)/L(Hα) $= 9.8 \pm 2.2$. Although this value is lower than the average (40 ± 9) for a large sample of objects (Elvis et al. 1984), it certainly falls within the observed range of values.

As an additional consistency check, the observed luminosity of the Balmer lines can be compared with that predicted from recombination theory given the ionizing luminosity. For this comparison, we chose Hβ instead of Hα, since the broad component of the former should be less affected by collisional enhancement than the latter. The total (narrow plus broad) dereddened Hβ luminosity is 4.2×10^{38} ergs s^{-1}; since case B recombination requires 8.6 Lyman continuum photons for each Hβ photon (Osterbrock 1989), the corresponding ionizing photon rate, assuming a covering factor of unity, is 8.8×10^{50} s^{-1}. This observed rate, however, is much larger than the rate inferred from interpolation of the spectral energy distribution ($\sim 1 \times 10^{50}$ s^{-1}; § 4.3.1). There are three possible explanations for this discrepancy: (1) a large fraction of the UV luminosity is obscured from direct view, (2) the shape of the unobserved EUV continuum differs drastically from the simple power law we assumed, or (3) photoionization by the featureless continuum provides only a small fraction to the total excitation of the gas. In view of the rough consistency between the observed emission-line spectrum and that predicted by photoionization models, the first two possibilities seem more plausible than the third. Note that if the ionizing luminosity has been substantially underestimated, then the sizes of the emission-line regions derived in the preceding two sections will be larger than quoted.

4.4. *Mass of Central Object and Bolometric Luminosity*

If one assumes that the line-of-sight velocity dispersion of the broad emission lines arises from gravitational motion, the mass of the central object can be derived once the average distance between the central source and the emitting clouds is known. Approximating the three-dimensional velocity dispersion by FWZI/4 (e.g., Wandel & Yahil 1985) and assuming that the average line widths of Lyα, C IV, and Mg II ($\langle$FWZI$\rangle \approx 10{,}000$ km s^{-1}) are representative, we find $M \approx (0.7\text{–}3) \times 10^6\ M_\odot$ for $r_{\rm BLR} = 0.001$–0.004 pc. From stellar velocity dispersion measurements, Keel (1989) obtained an upper limit of $2 \times 10^7\ M_\odot$ for the central mass. The derived mass and the BLR size indicate an extremely high mass density for the central region: $(1\text{–}20) \times 10^{13}\ M_\odot$ pc^{-3}. For comparison, the highest mass density thus far obtained from direct dynamical measurements is that of the active nucleus in NGC 4258 ($> 4 \times 10^9\ M_\odot$ pc^{-3}; Miyoshi et al. 1995). The inferred central density in M81 provides supporting, albeit indirect, evidence of a nonstellar origin for its nuclear activity.

It is worth noting that Fabbiano (1988) obtained a substantially smaller value for the central mass ($< 10^4$–$10^5\ M_\odot$) by fitting an accretion disk model to the soft X-ray spectrum taken with the *Einstein* satellite in 1979. In addition to being in an atypically low state in its X-ray emission (Petre et al. 1993; § 4.5), M81 also had an unusually steep soft X-ray spectrum at that epoch. Neither of these properties has since been observed in M81, and no adequate explanation for them has yet been advanced (Petre et al. 1993). Thus, it is difficult to evaluate the significance of the discrepancy between our mass estimate and that of Fabbiano, which, in any event, is very model dependent. FS, using essentially the same procedure adopted here, also obtained a somewhat smaller mass [$M = (3\text{–}8) \times 10^5\ M_\odot$]. The key difference is that FS assumed that the velocities implied by the broad Hβ emission line were typical of all BLR clouds, whereas we find that the permitted UV lines have much larger line widths than Hβ (§ 4.3.2). Adopting the formalism proposed by Wandel & Yahil (1985), FS found a BLR size (0.0013–0.0036 pc) that agrees surprisingly well with the values calculated here.

We can estimate the bolometric luminosity of the nucleus from the spectral energy distribution presented in § 4.2. Assuming that the 10 μm flux is entirely from the nucleus, we find a bolometric luminosity of $L_{\rm bol} = 9.3 \times 10^{40}$ ergs s^{-1}, or $2.4 \times 10^7\ L_\odot$. Since $M \approx (0.7\text{–}3) \times 10^6\ M_\odot$, $L_{\rm bol}/L_{\rm Edd}$ is only $\sim (2\text{–}10) \times 10^{-4}$. For an accretion efficiency of ~ 0.1, the implied accretion rate is $1.7 \times 10^{-5}\ M_\odot$ yr^{-1}. M81 could easily have maintained its current level of activity, if not even a slightly higher one in the past, over the entire history of the universe.

[5] We mention in passing that the models predict a ratio of He II λ4686 to (narrow) Hβ of $\sim$0.13–0.16, close to the observed ratio of 0.09 (Table 2). This implies that our adopted reddening correction is likely to be reasonably accurate.

4.5. *Variability*

Variability of the continuum and broad emission lines certainly represents one of the earmark properties of AGNs, with the level of variability generally increasing for sources of lower luminosity (Barr & Mushotzky 1986). In this respect, it is quite surprising that we find no evidence of variability in the broad Hα flux of M81 (§ 3.2), confirming and strengthening a similar conclusion reached by FS based on data covering only 3 yr. In fact, FS remarked that the Hα line looks qualitatively similar in spectra taken in 1978–1979 (Tonry & Davis 1979; Peimbert & Torres-Peimbert 1981), and unpublished spectra obtained in 1981 by one of us (A. V. F.) with the Palomar 1.5 m reflector look comparable as well. Thus, we conclude that the line flux has remained roughly constant for the past 15 yr.[6] Although it could be argued that our long-term monitoring is not sensitive to variability on short timescales, the long baseline of our observations certainly should have detected such "flares" had they been present at a level $\gtrsim 20\%$ above the average.

Fabbiano (1988) found some evidence for rapid ($\sim$minutes) soft X-ray variability in the nucleus of M81, but the statistical significance was not high. Although *EXOSAT* apparently detected extremely rapid ($\sim$600 s) soft X-ray variability (Barr et al. 1985), the null detection in more recent observations (Petre et al. 1993) casts doubt on the reality of the result (R. Mushotzky 1995, private communication). In contrast, long-timescale ($\sim$years) X-ray variability was detected (Petre et al. 1993). M81 was in an unusually low state during 1979: its 2–10 keV flux was about a factor of 10 lower than generally observed since then (Petre et al. 1993). Yet, as evidenced by the light curve of broad Hα, the BLR probably did not respond to this drastic continuum variation. We do not have an explanation for this behavior.

4.6. *The Physical Nature of LINERs and Low-Luminosity Seyfert Nuclei*

The collective evidence presented in this study demonstrates that photoionization by a nonstellar continuum most likely provides the dominant source of excitation for the LINER nucleus in M81. Thus, M81 hosts a genuine low-luminosity AGN. The nucleus of M81 in many ways resembles other LINERs showing broad Hα emission, and the results presented here may be applicable, in general, to this class of objects. For instance, we pointed out in § 4.3.2 that several other LINERs with limited UV spectroscopic information apparently show a similar pattern of low excitation and low density as deduced for the BLR of M81. Additionally, as Mushotzky (1993) first remarked, the small handful of LINERs thus far detected in X-rays have values of α_{ox} that are significantly lower than those of luminous AGNs, suggesting that the spectral energy distributions of LINERs tend to be X-ray bright relative to the optical or UV. Since Mushotzky (1993) used large-aperture *IUE* measurements to determine α_{ox}, his values are likely to be upper limits; the true values will be even lower once the uncontaminated UV continua of more LINERs are measured properly with the *HST*. A final similarity concerns the X-ray variability properties. Absence of rapid variability appears to be a generic trait among several LINERs observed with *ROSAT* (Mushotzky 1993; Reichert, Mushotzky, & Filippenko 1994), while changes in the X-ray luminosity over long timescales are not uncommon (Reichert et al. 1994).

These X-ray and UV properties need not be restricted solely to LINERs, but rather may be generic manifestations of low-level activity in most accretion-powered galactic nuclei. M51, which contains a low-luminosity Seyfert 2 nucleus, also emits an unusually large proportion of its power in X-rays ($\alpha_{ox} < 0.8$; Mushotzky 1993). The same can be said for the weak Seyfert 1 nucleus of NGC 1566 (Kriss et al. 1991). It is intriguing to note that the UV spectra of both M51 (Ellis et al. 1982) and NGC 1566 (Kriss et al. 1991) indicate a rather low ionization parameter. To this body of evidence we add NGC 4258, classified as a low-luminosity Seyfert 1 galaxy by Ho et al. (1996): its UV spectrum (Ellis et al. 1982), although highly uncertain, again suggests low ionization. It is plausible that most galactic nuclei displaying low-level activity, regardless of whether they are LINERs or Seyfert nuclei, share the same basic physical processes, and that the accretion rate is the fundamental parameter controlling their observed properties. (As a counterexample to this trend, we note that the Seyfert 1 nucleus of NGC 4395 has a fairly normal ionization level; Filippenko, Ho, & Sargent 1993.)

We do not suggest that other mechanisms previously advanced to explain LINERs (e.g., shock heating, Dopita 1995; hot stars, Terlevich & Melnick 1985, Shields 1994; composite photoionization plus shocks, Contini 1995) play no role in the excitation of the nucleus of M81. Clearly, shocks must accompany the highly supersonic motions of the line-emitting clouds, and star formation must be occurring at some level. Our proposition is that in M81, and, by analogy, in other similar objects, photoionization is the *dominant* excitation source, and that the ionizing radiation is analogous to that conventionally studied in luminous, "classical" AGNs. Whether the ultimate energy source in AGNs derives from stellar or nonstellar processes remains a topic of discussion (e.g., Heckman 1991; Terlevich et al. 1992; Filippenko 1992) and is not the subject of this study.

5. SUMMARY

We present an extensive discussion of the physical conditions and excitation of the LINER nucleus in M81. The analysis combines optical spectra from ground-based observations, archival *HST* spectra, published X-ray results, and various additional measurements at other wavelengths. The principal results can be summarized as follows:

1. The featureless UV continuum, most likely of nonstellar origin, has been detected definitively for the first time in M81. The slope of the continuum between $\sim$1200 and 3000 Å is significantly steeper ($f_\nu \propto \nu^{-2.0\pm0.3}$) than that observed in luminous AGNs, and the "big blue bump," commonly seen in luminous sources, is absent. The "small blue bump" due to Balmer continuum and Fe II emission is detected.

2. The overall spectral energy distribution of the nucleus of M81 differs substantially from those of luminous AGNs.

[6] After this paper was submitted, we learned that *HST* observations of the nucleus of M81 taken in 1995 March (Bower et al. 1996) showed that the broad component of Hα developed a double-peaked profile qualitatively resembling similar instances seen in NGC 1097 (Storchi-Bergmann, Baldwin, & Wilson 1993) and in Pictor A (Halpern & Eracleous 1994).

The main difference lies in the weakness of the UV continuum relative to the X-rays. We suggest that this could be a generic property of galactic nuclei with low-level activity.

3. Within the limitations of simple single-zone photoionization models, the observed emission-line spectrum broadly agrees with the predicted spectrum, suggesting that photoionization by a nonstellar continuum provides the dominant energy source and that M81 is a genuine low-luminosity AGN. However, the observed spectral energy distribution accounts for only $\sim 10\%$ of the ionizing photon budget inferred from the line luminosity. We suggest that a substantial fraction of the continuum is obscured along the line of sight to the observer; alternatively, most of the ionizing luminosity must be emitted in the EUV region.

4. Detailed properties have been derived for the regions emitting narrow and broad lines. The NLR is characterized by velocities (FWHM) of 200–1000 km s^{-1}, a large range of electron densities (a few times 10^2–10^7 cm^{-3}), a density gradient increasing toward the center, $\log U \approx -3.3$, characteristic dimensions ranging from less than 1 to several parsecs, and approximately solar abundances. The electron temperatures derived for the O^{++} and N^+ regions are fully consistent with those expected for photoionized nebulae. The properties of the BLR are more uncertain, and we estimate that $\log U \lesssim -2.8$, $n \approx 10^9$–10^{10} cm^{-3}, and $r \approx 0.001$–0.004 pc. The broad lines typically have FWHM $\approx$ 2500 km s^{-1}, but extreme velocities of $\sim$10,000 km s^{-1} (FWZI) are present.

5. Combining the velocities of the broad lines with the size estimate of the BLR, we derive a central mass of $M \approx (0.7\text{–}3) \times 10^6\ M_\odot$. For the observed bolometric luminosity, $L_{\rm bol}/L_{\rm Edd} \approx (2\text{–}10) \times 10^{-4}$.

6. The broad component of the Hα emission line has not varied appreciably for the past 15 yr, although long-timescale X-ray variability has been reported.

7. Several LINERs and low-luminosity Seyfert nuclei have properties similar to those observed in M81. We suggest that the accretion rate is the fundamental parameter controlling the level of activity in galactic nuclei.

We thank the technical staff at Palomar and Lick Observatories for their assistance with the ground-based observations. The starlight subtraction of the ground-based spectra was greatly expedited using software adapted from a program written by Hans-Walter Rix. Chien Peng helped develop the code used for deblending spectral lines. We are very grateful to Jerry Kriss and Zlatan Tsvetanov for bringing to our attention a calibration problem in the G130H spectrum and for kindly making available to us the recalibrated version of the spectrum. Howard Bushouse and Anuradha Koratkar at the Space Telescope Science Institute also offered useful advice on the calibration of the FOS data. Correspondence with Min Yun, Richard Mushotzky, and Michele Kaufman helped clarify some observational issues, and Harry Ferguson generously communicated his unpublished UV spectrum of NGC 3610. An anonymous referee and Chris McKee provided constructive criticism that improved the presentation of the paper. Support for this work was provided by NASA through grants AR-4911.01-92A and AR-5291.01-93A from the Space Telescope Science Institute, which is operated by the AURA, Inc., under NASA contract NAS5-26555. Additional financial support was obtained by NSF grant AST-8957063 to A. V. F., and by NSF grants AST-8819792 and AST-9221365 to W. L. W. S.

APPENDIX

ULTRAVIOLET INTERSTELLAR ABSORPTION LINES

A number of interstellar absorption lines are present in the UV spectra. Unambiguously detected species include Lyα, S I, Si II, Fe II, Mg II and Mg I (Table 3); there may be additional lines present, although the quality of the data makes their identification uncertain. It is apparent from column (5) of Table 3 that the measured heliocentric velocities of the tabulated lines do not show internal consistency, suggesting that the zero points of the wavelength scale of the G130H and G270H spectra may be incorrect. Specifically, the lines of the G130H spectrum have much larger velocities than those of the G270H spectrum. If we demand that the narrow geocoronal Lyα line have zero velocity, then the G130H wavelength scale must be shifted by -91 km s^{-1}, or approximately 0.4 of a diode. Likewise, if we assume that the Mg II doublet has the same velocity as Lyα (see argument below), then the wavelength scale of the G270H spectrum must be shifted by $+112$ km s^{-1}, equivalent to approximately half a diode. Although the magnitudes of these offsets are larger than usual (Kinney 1994), they are consistent with a recent determination of the offset resulting from misalignment of the FOS filter wheel (A. Koratkar 1995, private communication). Column (6) of Table 3 lists the corrected heliocentric velocities.

With our adopted wavelength zero point, the observed velocities span between 120 and 220 km s^{-1}. An FOS spectrum of SN 1993J in M81 (Jeffery et al. 1994) also shows several interstellar absorption lines with a similar range of velocities. Because M81 has a small radial velocity, it is uncertain whether the absorption arises from our Galaxy or from M81 itself, especially when one considers the complex kinematics of the gas (Yun, Ho, & Lo 1993). Both H I emission (Hulsbosch & Wakker 1988) and absorption (M. Yun 1995, private communication) with velocities similar to those reported here are seen in the direction of M81, although most of the gas lies outside of the nucleus (M. Yun 1995, private communication). The Lyα absorption line is clearly saturated; the enormous width of the line arises from the damping wings of the absorption profile. A rough estimate of the column density yields $N(\text{H I}) \approx 1.6 \times 10^{20}$ cm^{-2}. Using the standard conversion $N(\text{H}) = 5.9 \times 10^{21}\ E(B-V)$ cm^{-2} (Spitzer 1978), this corresponds to a reddening of $E(B-V) = 0.03$ mag, in reasonable agreement with the Galactic contribution of 0.038 mag (Burstein & Heiles 1984). The Mg II doublet has a ratio close to unity, indicating a large optical depth. The upper limit for the Doppler parameter (after correcting for instrumental resolution) is $\sim$160 km s^{-1}. Assuming that the logarithmic portion of the curve of growth is applicable, $N(\text{Mg II}) = 9.2 \times 10^{15}$ cm^{-2}. Similarly, the equivalent width of the weak Mg I λ2853 line implies $N(\text{Mg I}) = 2.2 \times 10^{13}$ cm^{-2}, or that most of the Mg is singly ionized. The above column density estimates indicate that the absorbing material has roughly solar Mg abundance: $\log [N(\text{Mg II})/N(\text{H I})] = -4.2$, only slightly

TABLE 3

ABSORPTION LINES IN M81

Line	λ_{vac}[a] (Å)	λ_{obs} (Å)	W_λ[b] (Å)	$cz_\odot$[c] (km s^{-1})	$cz_\odot$[d] (km s^{-1})
Lyα	1215.67	1216.96±0.10	7.5±2	276±25	185±25
S I	1224.54	1225.69±0.07	1.17±0.19	284±17	193±17
S I	1233.35	1234.22±0.07	7.24±1.89	211±17	120±17
Si II	2344.92	2345.27±0.09	0.93±0.15	45±12	157±12
Fe II	2374.46	2374.40±0.10	2.42±0.20	8±13	120±13
Fe II	2382.77	2383.56±0.10	1.74±0.40	99±13	211±13
Fe II	2586.65	2587.60±0.30	1.49±0.30	110±35	222±35
Fe II	2600.17	2600.92±0.10	2.05±0.10	86±12	198±12
Mg II	2796.35	2797.09±0.05	6.4±1	79±5	191±5
Mg II	2803.53	2804.17±0.05	6.4±1	68±5	180±5
Mg I	2852.96	2853.77±0.10	0.91±0.10	85±11	197±11

[a] From Morton 1991.

[b] Equivalent widths measured with respect to the local "continuum" level; for Lyα and Mg II, they are measured relative to the unabsorbed, intrinsic emission profile (see text).

[c] Heliocentric radial velocity as measured in original spectra.

[d] Heliocentric radial velocity after correcting for offsets in the zero point of the wavelength scale.

larger than the solar value of log $[N(\mathrm{Mg})/N(\mathrm{H})] = -4.41$ (Morton 1991). This result, unless completely fortuitous, reinforces our belief that both the Lyα *and* Mg II absorption lines originate from the same absorbing material, and, accordingly, that they should have roughly the same velocity. As explained above, the zero point of the wavelength scale of the G130H and G270H spectra were adjusted based on this consideration.

REFERENCES

Barr, P., Giommi, P., Wamsteker, W., Gilmozzi, R., & Mushotzky, R. F. 1985, BAAS, 17, 608
Barr, P., & Mushotzky, R. F. 1986, Nature, 320, 421
Bartel, N., et al. 1982, ApJ, 262, 556
Barvainis, R. 1993, ApJ, 412, 513
Bash, F. N., & Kaufman, M. 1986, ApJ, 310, 621
Bertola, F., Capaccioli, M., Holm, A. V., & Oke, J. B. 1980, ApJ, 237, L65
Bietenholz, M. F., et al. 1996, ApJ, 457, 604
Bower, G. A., Heckman, T. M., Wilson, A. S., & Richstone, D. O. 1996, in The Physics of LINERs in View of Recent Observations, ed. M. Eracleous et al. (San Francisco: ASP), in press
Bruzual A, G., Peimbert, M., & Torres-Peimbert, S. 1982, ApJ, 260, 495
Burstein, D., Bertola, F., Buson, L.M., Faber, S. M., & Lauer, T. R. 1988, ApJ, 328, 440
Burstein, D., & Heiles, C. 1984, ApJS, 54, 33
Cardelli, J. A., Clayton, G. C., & Mathis, J. S. 1989, ApJ, 345, 245
Contini, M. 1995, preprint
Crane, P. C., Giuffrida, B., & Carlson, J. B. 1976, ApJ, 203, L113
de Bruyn, A. G., Crane, P. C., Price, R. M., & Carlson, J. 1976, A&A, 46, 243
De Robertis, M. M., & Osterbrock, D. E. 1986, ApJ, 301, 727
De Robertis, M. M., & Shaw, R. A. 1990, ApJ, 348, 421
de Vaucouleurs, G., de Vaucouleurs, A., Corwin, H. G., Jr., Buta, R. J., Paturel, G., & Fouqué, R. 1991, Third Reference Catalogue of Bright Galaxies (New York: Springer)
Dopita, M. A. 1995, in The Analysis of Emission Lines, ed. R. E. Williams & M. Livio (Cambridge: Cambridge Univ. Press), in press
Dopita, M. A., & Sutherland, R. S. 1996, ApJS, 102, 161
Dressler, A., & Richstone, D. O. 1990, ApJ, 348, 120
Ellis, R. S., Gondhalekar, P. M., & Efstathiou, G. 1982, MNRAS, 201, 223
Elvis, M., Soltan, A., & Keel, W. C. 1984, ApJ, 283, 479
Elvis, M., et al. 1994, ApJS, 95, 1
Fabbiano, G. 1988, ApJ, 325, 544
———. 1996, in The Physics of LINERs in View of Recent Observations, ed. M. Eracleous et al. (San Francisco: ASP), in press
Ferguson, H. C., & Davidsen, A. F. 1993, ApJ, 408, 92
Ferland, G. J., Peterson, B. M., Horne, K., Welsh, W. F., & Nahar, S. N. 1992, ApJ, 387, 95
Filippenko, A. V. 1985, ApJ, 289, 475
———. 1989, in Active Galactic Nuclei, ed. D. E. Osterbrock & J. S. Miller (Dordrecht: Kluwer), 495
———. 1992, in Physics of Active Galactic Nuclei, ed. W. J. Duschl & S. J. Wagner (Berlin: Springer), 345
———. 1993, in The Nearest Active Galaxies, ed. J. Beckman, L. Colina, & H. Netzer (Madrid: CSIC Press), 99
Filippenko, A. V., & Halpern, J. P. 1984, ApJ, 285, 458
Filippenko, A. V., Ho, L. C., & Sargent, W. L. W. 1993, ApJ, 410, L75
Filippenko, A. V., & Sargent, W. L. W. 1985, ApJS, 57, 503
———. 1988, ApJ, 324, 134 (FS)
———. 1989, ApJ, 342, L11
Forbes, D. A., Ward, M. J., DePoy, D. L., Boisson, C., & Smith, M. S. 1992, MNRAS, 254, 509
Fosbury, R. A. E., Snijders, M. A. J., Boksenberg, A., & Penston, M. V. 1981, MNRAS, 197, 235
Francis, P. J., Hewett, P. C., Foltz, C. B., Chaffe, F. H., Weymann, R. J., & Morris, S. L. 1991, ApJ, 373, 465
Freedman, W. L., et al. 1994, ApJ, 427, 628
Goodrich, R. W., & Keel, W. C. 1986, ApJ, 305, 148
Grandi, S. A. 1981, ApJ, 251, 451
Guilbert, P. W., & Rees, M. J. 1988, MNRAS, 233, 475
Halpern, J. P., & Eracleous, M. 1994, ApJ, 433, L17
Halpern, J. P., & Filippenko, A. V. 1984, ApJ, 285, 475
Heckman, T. M. 1980, A&A, 87, 152
———. 1991, in Massive Stars in Starbursts, ed. N. Walborn & C. Leitherer (Cambridge: Cambridge Univ. Press), 289
Ho, L. C., Filippenko, A. V., & Sargent, W. L. W. 1993, ApJ, 417, 63
———. 1995, ApJS, 98, 477
———. 1996, in preparation
Hulsbosch, A. N. M., & Wakker, B. P. 1988, A&AS, 75, 191
Jeffery, D. J., et al. 1994, ApJ, 421, L27
Keel, W. C. 1983, ApJ, 269, 466
———. 1989, AJ, 98, 195
Keel, W. C., & Windhorst, R. A. 1991, ApJ, 383, 135
Kinney, A. L. 1994, Faint Object Spectrograph Instrument Handbook, Version 5.0 (Baltimore: STScI)
Kinney, A. L., Bohlin, R. C., Calzetti, D., Panagia, N., & Wyse, R. F. G. 1993, ApJS, 86, 5
Kollatschny, W., & Fricke, K. J. 1984, A&A, 135, 171
Kriss, G. A., Canizares, C. R., & Ricker, G. R. 1980, ApJ, 242, 492
Kriss, G. A., Hartig, G. F., Armus, L., Blair, W. P., Caganoff, S., & Dressel, L. 1991, ApJ, 377, L13
Krolik, J. H., Horne, K., Kallman, T. R., Malkan, M. A., Edelson, R. A., & Krisss, G. A. 1991, ApJ, 371, 541
Kwan, J. 1984, ApJ, 283, 70
Kwan, J., & Krolik, J. H. 1981, ApJ, 250, 478
Lawrence, A., Ward, M., Elvis, M., Fabbiano, G., Wilner, S. P., Carleton, N. P., & Longmore, A. 1985, ApJ, 291, 117
Malkan, M. A. 1988, in Adv. Space Res., 8(2), 49
Malkan, M. A., & Sargent, W. L. W. 1982, ApJ, 254, 22
Mazzarella, J. M., & Boroson, T. A. 1993, ApJS, 85, 27
Miller, J. S., & Stone, R. P. S. 1987, Lick Obs. Tech. Rep. 48
———. 1993, Lick Obs. Tech. Rep. 66
Miyoshi, M., Moran, J., Herrnstein, J., Greenhill, L., Nakai, N., Diamond, P., & Inoue, M. 1995, Nature, 373, 127
Morton, D. C. 1991, ApJS, 77, 119
Mushotzky, R. F. 1982, ApJ, 256, 92
———. 1993, in The Nearest Active Galaxies, ed. J. Beckman, L. Colina, & H. Netzer (Madrid: CSIC Press), 47
Mushotzky, R. F., & Ferland, G. J. 1984, ApJ, 278, 558
Mushotzky, R. F., & Wandel, A. 1989, ApJ, 339, 674

Oke, J. B., & Gunn, J. E. 1982, PASP, 94, 586
Osterbrock, D. E. 1989, Astrophysics of Gaseous Nebulae and Active Galactic Nuclei (Mill Valley: University Science Books)
Peimbert, M., & Torres-Peimbert, S. 1981, ApJ, 245, 845
Peterson, B. M. 1993, PASP, 105, 247
Petre, R., Mushotzky, R. F., Serlemitsos, P. J., Jahoda, K., & Marshall, F. E. 1993, ApJ, 418, 644
Phillips, M. M., Jenkins, C. R., Dopita, M. A., Sadler, E. M., & Binette, L. 1986, AJ, 91, 1062
Reichert, G. A., Branduardi-Raymont, G., Filippenko, A. V., Mason, K. O., Puchnarewicz, E. M., & Wu, C.-C. 1992a, ApJ, 387, 536
Reichert, G. A., Mushotzky, R. F., & Filippenko, A. V. 1994, in The First ROSAT Science Symposium, ed. E. M. Schlegel & R. Petre (New York: AIP), 85
Reichert, G. A., Mushotzky, R. F., Petre, R., & Holt, S. S. 1985, ApJ, 296, 69
Reichert, G. A., Puchnarewicz, E. M., Filippenko, A. V., Mason, K. O., Branduardi-Raymont, G., & Wu, C.-C. 1992b, in Relationships Between Active Galactic Nuclei and Starburst Galaxies, ed. A. V. Filippenko (San Francisco: ASP), 277
———. 1993, in The Nearest Active Galaxies, ed. J. Beckman, L. Colina, & H. Netzer (Madrid: CSIC Press), 85
Reichert, G. A., Puchnarewicz, E. M., & Mason, K. O. 1990, in Evolution in Astrophysics: *IUE* in the Era of New Space Missions, ed. E. Rolfe (Noordwijk: ESA), 535
Rickard, L. J., & Harvey, P. M. 1984, AJ, 89, 1520
Rieke, G. H., & Lebofsky, M. J. 1978, ApJ, 220, L37
Rosa, M. R. 1994, FOS Instrument Science Report CAL/FOS-127
Seaton, M. J. 1978, MNRAS, 185, 5P
Shields, J. C. 1994, in Violent Star Formation from 30 Doradus to QSOs, ed. G. Tenorio-Tagle (Cambridge: Cambridge Univ. Press), 353
Shuder, J. M., & Osterbrock, D. E. 1981, ApJ, 250, 55
Spitzer, L., Jr. 1978, Physical Processes in the Interstellar Medium (New York: Wiley)
Stauffer, J. R. 1982, ApJ, 262, 66
Storchi-Bergmann, T., Baldwin, J. A., & Wilson, A. S. 1993, ApJ, 410, L11
Storchi-Bergmann, T., Kinney, A. L., & Challis, P. 1995, ApJS, 98, 103
Terlevich, R., & Melnick, J. 1985, MNRAS, 213, 841
Terlevich, R., Tenorio-Tagle, G., Franco, J., & Melnick, J. 1992, MNRAS, 255, 713
Tonry, J., & Davis, M. 1979, AJ, 84, 1511
Turner, J. L., & Ho, P. T. P. 1994, ApJ, 421, 122
Turner, T. J., & Pounds, K. A. 1989, MNRAS, 240, 833
Véron, P. 1979, A&A, 78, 46
Wandel, A., & Yahil, A. 1985, ApJ, 295, L1
Weedman, D. W. 1976, ApJ, 208, 30
Whittle, M. 1985, MNRAS, 216, 817
Willner, S. P., Elvis, M., Fabbiano, G., Lawrence, A., & Ward, M. J. 1985, ApJ, 299, 443
Wills, B. J., Netzer, H., & Wills, D. 1985, ApJ, 288, 94
Yun, M. S., Ho, P. T. P., & Lo, K.-Y. 1993, ApJ, 411, L17

Note added in proof.—In § 4.3.2, we argued that the Mg^+ zone in the BLR has a density $\lesssim 2 \times 10^9$ cm^{-3}. Our conclusion, which was based on the mistaken impression that C II] λ2326 and Mg II λ2800 have similar line widths, is unfounded, since C II] is in fact *narrower* than Mg II (Table 2, Fig. 10).